Wave Propagation in Pulmonary Circulation: Effect of Pulmonary Hypertension due to Sickle Cell Disease

BY

ANDREA CARMIGNOTTO
Laurea, Politecnico di Milano, Milan, Italy, 2015

THESIS

Submitted as partial fulfillment of the requirements
for the degree of Master of Science in Bioengineering
in the Graduate College of the
University of Illinois at Chicago, 2017

Chicago, Illinois

Defense Committee:
Thomas J. Royston, Chair and Advisor
Dieter Klatt
Pasquale Vena, Politecnico di Milano

To my "little" brother Riccardo,
who always gives me the strength to go on
with his support and love.

ACKNOWLEDGMENTS

First and foremost, I express my deepest gratefulness and sincere acknowledgement to my advisor, Dr. Thomas J. Royston, for his teaching and supervision through each step of this work. I am particularly grateful to Prof. Pasquale Vena and Prof. Jose Felix Rodriguez Matas, for their precious comments and insights, and their support from back home. I would like to thank Dr. Dieter Klatt as a professor and committee member, for his patience and valuable suggestions.

The financial support of the National Institutes of Health (Grant # EB012142) and the National Science Foundation (Grant # 1302517) is acknowledged.

A special thanks must be addressed to Brian Henry, without whom I couldn't have achieved my goal. His encouragement, support, knowledge, and infinite patience have been fundamental for me and helped me going on with my research.

I would also like to thank my friends Cecilia and Lorenzo. We went through every day together, supporting each other.

Last but not least, I thank my parents and my brother for always supporting me and being there for me. They have been my strength away from home; my dad who has always been blunt to me, pushing me to face difficulties without giving up; my mom who is always able to make me feel home with her love; my younger brother who despite the distance was always close to me.

AC

TABLE OF CONTENTS

TABLE OF CONTENTS (continued)

LIST OF TABLES

LIST OF FIGURES

LIST OF FIGURES (continued)

LIST OF ABBREVIATIONS

6MWT	6-Minute Walk Test
CFD	Computational Fluid Dynamics
CT	Computerized Tomography
FE	Finite Element
GUI	Graphic User Interface
mPap	Main Pulmonary Artery Pressure
NO	Nitric Oxide
PAH	Pulmonary Arterial Hypertension
PAWP	Pulmonary Artery Wedge Pressure
PH	Pulmonary Hypertension
PVR	Pulmonary Vascular Resistance
RAP	Right Atrial Pressure
RHC	Right Heart Catheterization
RV	Right Ventricle
SMC	Smooth Muscle Cells
TRV	Tricuspid Regurgitation Peak Velocity
TVI_{RVOT}	Time-Velocity Integral Right Ventricular Outflow Tract

WHO	World Health Organization

SUMMARY

Sickle-cell disease (SCD) is a common disorder, which affects more than two million people worldwide, with approximatively 100000 cases in the United States. One of the main complications of its progression is pulmonary hypertension (PH), a pathological condition highly related to patients' death, characterized by mean pulmonary artery pressure (mPap) higher than 25 mm Hg at rest. The gold-standard for mPap measurement, thus for PH diagnosis, is right heart catheterization (RHC). RHC is an invasive, technically difficult, and expensive technique, which exposes patients to high risks (infection, bleeding, …). Although non-invasive techniques, such as echocardiography, have been shown to be suitable to obtain diagnostically relevant information, RHC is still mandatory to establish PH diagnosis and gaining insight into the disease progression. Computational hemodynamics models can play a fundamental role in this clinical background, which ranges from monitoring disease progression and/or response to treatment, to planning intervention and integrating experimental data for diagnostic purposes. In this work, the pulmonary circulation has been modeled as a one-dimensional branching waveguide with the purpose of simulating the pressure wave propagation and the effect of SCD and PH. A frequency-domain analytical model has been developed, based on the models proposed by Wiener [1] and Olufsen [2]. Three main parts comprise the present work:

1. A preliminary study, in which the analytical model has been compared to a finite element model;
2. A pulse wave simulation, in which a pressure pulse has been simulated via superposition of different harmonics;

3. Pulmonary hypertension simulation, in which structural and mechanical changes have been introduced in the model with the aim of simulate the effect of the pathology.

In the preliminary study, the analytical model has been validated since the comparison with the finite element model showed a good agreement in the results. The pulse wave simulation shows the versatility of the approach chosen for the analytical model. In fact, the frequency-domain analytical model was able to give all pieces of information necessary to reconstruct the arterial pulse wave in the time domain. The results of the pathology simulation have shown changes in pressure distribution along the arterial tree and changes in the phase velocity, which can be relevant from a clinical perspective.

The developed model turned out to be a versatile and suitable tool for different application, that can be further developed with the aim of obtaining diagnostically relevant information and a better knowledge of disease processes related to pathologies, such as pulmonary hypertension.

CHAPTER 1

INTRODUCTION

1.1 Cardiovascular System in Humans

The cardiovascular system is in charge of providing nutrients and oxygen to all tissues, and of getting rid of wastes[3]; three parts mainly compose it:

1. The blood, the medium of transport and exchange;
2. The heart, a pump that moves blood against a pressure gradient;
3. The vascular system, a series of tubes to carry the blood.

Blood is a fluid, composed by several types of cells or fragments and has three main functions[4]. The first one is a transport function: blood carries oxygen and carbon dioxide from/to lungs to/from tissues, nutrients from the gastrointestinal system to tissues, waste products to the kidneys, lungs and skin, and hormones all around the body. Secondly, its action is aimed at the regulation of pH, via buffers contained in it, and body temperature, via the watery part of plasma. Last, but not least, blood has a protective function: clotting cascade prevents excessive loss in blood volume, white blood cells protect the body from pathogens, and so on. The “extracellular matrix” occupies 55 percent of the total blood volume and constitutes the liquid part of it, called plasma; it is about 91.5 percent water, with the remaining fraction constituted by solutes, such as protein, electrolytes, and gases. Cells and cells fragment are the so called formed elements, composed by erythrocytes, leukocytes, and platelets, which are about 45 percent of the total blood volume. Red blood cells, another name to refer to erythrocytes, are responsible for carrying oxygen in blood. They are biconcave discs, characterized by a diameter

of 7-8 μm, which can easily deform and squeeze without rupture, thanks to a resistant, but flexible plasma membrane: this feature is fundamental for the passage through narrow capillaries of microcirculation, and can be affected by specific pathologies. No nucleus is present in red blood cells. The oxygen-carrying function is allowed by hemoglobin, a globular protein contained in the erythrocyte's cytosol; globin, a protein of four polypeptide chains, and four hemes group constitutes hemoglobin. The center of each hemes group is characterized by the presence of an Fe^{2+} ion, able to reversibly bind to oxygen. Other than the transport of oxygen, hemoglobin also carry carbon dioxide, a waste product from the cellular metabolism. Nitric oxide (NO) is another chemical able to bind to hemoglobin: NO is released by endothelial cells, binds to hemoglobin, and if released causes vasodilation, namely the relaxation of smooth muscle cells. Leukocytes, also called white blood cells, are the responsible of protection against pathogens via phagocytosis or immune response. They are classified as granular, which include neutrophilis, eosinophilis, and basophilis, and agranular, including lymphocytes and monocytes. Platelets are fragments of megakaryocytes, cells coming from hemopoietin stem cells. An irregular disc shape with a diameter between 2-4 μm characterizes them; several vesicles are contained in their cytoplasm, but no nucleus: these vesicles contain chemicals that once released promote blood clotting. The heart is a muscle which constitutes the central organ of the cardiovascular system[5]. It is placed in the thoracic cavity, in an anatomical space in between the two lungs called the mediastinum. It is surrounded by the pericardium, a sac constituted by a serous layer and a fibrous layer, which fixes the heart to the diaphragm. Cardiac muscle is cone-shaped, with the apex pointing downward and the base in anteroposterior position. Roughly the heart is 12 cm long, 9 cm wide (as a maximum), and 6 cm thick; its weight varies in a range of 280 g – 340 g in men and 230 g – 280 g in women. The right heart and left heart are the two

elements that can be distinguished in the heart: the former drives the blood in the pulmonary circulation, the latter in the systemic circulation. In either side of the heart, two chambers can be identified, an atrium, the superior one, and a ventricle, the inferior one. The two atria and the two ventricles are respectively separated by the interatrial septum and the interventricular septum. The ventricular base presents two orifices, a posterior one (atrioventricular) and an anterior one (arteriosus). These two orifices differ in the kind of valves: semilunar valves (aortic and pulmonary) are present in the arteriosus orifice, while the atrioventricular is characterized by cusps valves (mitral and tricuspid). Cardiac valves opening is pressure driven in response to heart contraction or relaxation, and they ensure the unidirectionality of the blood flow, allowing the blood to go through and preventing the backflow. Heart exploits its main function pumping blood in vasculature, with a continuous cycle of contraction and relaxation. Heart contraction drives blood in systemic and pulmonary circulation, two routes arranged in series. Blood that receives oxygen in lungs, goes into the left heart, which in turn propels it into the systemic circulation. After passing through the tissues, right atrium receives blood with any oxygen left in it, which the right ventricle in turn pumps into the pulmonary circulation. Blood vessels are categorized in five main types: arteries, arterioles, capillaries, venules, and veins. Blood is transported from the heart to the periphery by arteries: near the heart one can recognize large and elastic arteries, which in turn branch into muscular medium-sized arteries. Medium-sized arteries then divide into small arteries, which in turn give rise to arterioles. Inside the tissues, arterioles branch further, dividing into capillaries. These small vessels constitute the exchange zone between blood and interstitial fluid: this is possible thanks to their thin walls, which in some cases present gaps that facilitate the nutrient passage (fenestrated capillaries, discontinuous capillaries). Venules arise within the tissue from the merging of groups of capillaries and in turn

convergent venules form veins; veins are larger blood vessels, aimed at return blood to the heart. In the wall of a blood vessel, one can recognize three layers, which differ for the tissue characteristics. These layers are also called tunics and from the inner to the outer are respectively:

- Tunica intima, an endothelial layer in direct contact with blood;
- Tunica media, constituted by smooth muscle and elastic tissue;
- Tunica adventitia, in which collagen and elastic fibers are widely present.

According to the type of blood vessel and the specific function, the composition of these three layers varies.

1.1.1 Pulmonary circulation

Pulmonary circulation is fundamental for blood oxygenation: it is the pathway that leads the deoxygenated blood, pumped from the right ventricle, to the alveoli, and that returns oxygenated blood to the left atrium. This system appears to closely follow the bronchial tree, either downward with arteries or upward with the venous side. The pulmonary trunk, or main pulmonary artery, exits the right ventricle and branches into right and left pulmonary arteries, respectively headed to the right and the left lung. The main pulmonary artery is about 3 cm in diameter, while left and right pulmonary artery diameter are smaller (maximum diameter = 1.5 cm)[6]. The main pulmonary artery pathway is continued by the left pulmonary artery, that generates an upper lobe and a lower lobe artery, after going over the left main stem bronchus. The former divides into the apicoposterior, anterior and lingular arteries, that further branch into a superior and inferior segmental artery; the latter gives rise to a superior, an anteromedial, a lateral, and a posterior basal segmental artery. The right pulmonary artery generates right upper

lobe artery and a right lower lobe artery, in correspondence of the main stem bronchus. Apical, posterior, and anterior segmental arteries arise from the right upper lobe artery; the lower lobe artery further branches into the following segmental arteries: apical, anterior, posterior, medial and lateral. A number of supranumerary vessels accompanies this conventional arterial pathway. These are vessels which branches perpendicularly from the parent arteries and does not follow any airway segment. Pulmonary veins pathways run parallel to the pulmonary artery and airways. In the right upper lobe, major pulmonary veins follow the superior vena cava. The right upper pulmonary vein generally arises from the right middle lobe vein and the upper lobe vein, and ends itself into the left atrium. On the contrary, a single pulmonary vein allows the drainage of the right inferior lobe in the left atrium. Similarly, one left upper pulmonary vein arises from the superior segment and the lingular veins. Although, the typical pattern of the drainage into the left atrium shows the presence of two left and two right pulmonary veins, the occurrence of independent veins draining in the left atrium is relevant. The network of blood vessels above described is characterized by low pressure: pulmonary arterial pressure varies from 10 to 25 mmHg, while pulmonary venous pressure is only 4 mmHg to 5 mmHg. This feature affects the properties of the vessels wall within the pulmonary circulation: for example the wall of large pulmonary arteries has been shown to be thinner than the aorta one [7]. Taking into account arteries first, one can notice some interesting features in the composition of their wall. The adventitia of pulmonary arteries presents a loose organization and consists of extracellular matrix, interstitial cells like fibroblasts, a vasa vasorum and nerves; elastin and collagen fibers are seen too in this layer. Tunica intima composition changes from the proximal to distal arteries, according to whether or not elastic lamina is present and how much the degree of muscularity is; in fact, elastic lamina and smooth muscle cells mainly compose large elastic arteries. Going

away from the heart along the arteries, it can be noticed that the less the diameter is, the less smooth muscle cells are present and the more the tunica media is composed only by elastic lamina; in small distal arteries, elastic lamina may eventually disappear. Instead of all that, pulmonary vasculature tunica intima is comprised of endothelial cells and sub-endothelial interstitium.

TABLE 1-DATA ON THE PULMONARY ARTERIAL TREE [7]

Order	**Number of branches**	**Diameter [mm]**	**Length [mm]**	**End branches**
17	1.00	30.00	90.50	3.00e8
16	3.00	14.83	32.00	1.00e8
15	8.00	8.06	10.00	3.02e7
14	2.00e1	5.82	20.70	1.37e7
13	6.60e1	3.65	17.90	3.98e6
12	2.03e2	2.09	10.50	1.16e6
11	6.75e2	1.33	6.60	3.47e5
10	2.29e3	0.85	4.69	8.92e5
9	5.86e3	0.52	3.16	4.80e4
8	1.76e4	0.35	2.10	1.60e4
7	5.25e4	0.22	1.38	5.36e3
6	1.57e5	0.14	0.91	1.79e3
5	4.71e5	0.09	0.65	5.97e2
4	1.41e6	0.05	0.44	1.99e2
3	4.27e6	0.03	0.29	6.66e1
2	1.27e7	0.02	0.20	2.37e1
1	3.00e8	0.01	0.13	1.00

1.2 Sickle-Cell Disease

Sickle-cell disease is a common disorder worldwide. It is a disease arising at the cardiovascular level, but its effects are spread all around the organism. In common parlance, sickle-cell disease and sickle-cell anemia are often used as synonyms, even though this is inaccurate. The term sickle-cell disease considers all kind of genotypic mutations, while sickle-cells anemia refers only to the mutation of the β^s allele (HbSS): it represents the 70% of sickle-cell diseases, with the remaining fraction occupied mostly by HbSC disease[8]. Sickle-cell disease, usually referred to as HbS, is an autosomal recessive disease, triggered by mutation in the gene that encodes hemoglobin: the 17^{th} nucleotide of this gene presents adenosine instead of thymine, and the 6^{th} aminoacid in the β-globin chain is valine, instead of glutamic acid. A hydrophobic site appears in the deoxygenated HbS tetramer, leading to the crystallization of two Hb molecules via a binding between β_1 and β_2 chains. This leads to a polymer nucleus, that filling the erythrocyte, disrupts its architecture and flexibility, and implies dehydration. The sickle-shaped red blood cells become in this way less deformable and may be entrapped in microcirculation, causing acute vaso-occlusive pain. Other than HbS polymerization, microcirculation occlusion is triggered by inflammatory events: during inflammation, vascular endothelium becomes more adhesive for leucocytes and erythrocytes. Thus, rigid red blood cells interact with the more adhesive vascular endothelium, leading to ischemia due to vaso-occlusion. Because of ischemia, the blood flow needs to be restored, so reperfusion happens, which further injures tissues. This whole cycle of ischemia and reperfusion is damaging to the organism, since it triggers oxidative and inflammatory stress. Hemolytic anemia is the second development of a sickle-cell pathological case. Hemolysis consists in the rupture of the erythrocyte, with the consequent release in the blood flow of all its content; anemia is the reduction of red blood and Hb amount in blood, which

itself is one of the major causes of elevated cardiac output: a dilated ventricle is the consequence of this elevated cardiac output. Severe anemia is related with a reduction vascular resistance of both circulations. In sickle-cell patients with severe anemia, but without pulmonary hypertension, the pulmonary vascular resistance between 68 to 74 $dyn \cdot s \cdot cm^{-5}$, while in normal patients it is a between 80 and 120 $dyn \cdot s \cdot cm^{-5}$[9]. Another effect of severe anemia is the reduction of blood viscosity, which is opposes the effects of sickle-shaped red blood cells [10]. In fact, erythrocytes containing HbS are supposed to increase blood viscosity, but anemia effects far exceed this process: the net result is a decrease in blood viscosity in severe anemia cases [11]. Because of the lower vascular resistance and diastolic pressure, and increase vascular stiffness and stroke volume, patients show a high pulse pressure in either circulatory pathways, pulmonary and systemic. The intensity of hemolytic anemia has also been reported as correlated with pulmonary hypertension in three screening studies of HbS patients [12],[13],[14]. At the molecular level, the hemolysis of erythrocyte, and the release of Hb in the blood flow, has relevant consequences. Reactive oxygen species are generated by free plasma Hb, which strongly inhibits Nitric Oxide (NO) function; NO is a molecule secreted by endothelial cells and it is involved in the regulation of vasodilation. The inhibition of NO and the generation of reactive oxygen species alter blood redox balance and, as a consequence, impair endothelial function and promote proliferative vasculopathy. Moreover, free plasma Hb is degraded and release heme group. The presence of both Hb and heme in the blood stream stimulates platelets activation: coagulation is then triggered and the whole process can lead to pulmonary vascular thrombosis, which can in turn cause pulmonary hypertension.

Starting from the considerations reported above, the main courses of sickle-cell disease include:

- Acute pain: acute pain is mainly related to the vaso-occlusion process and it is one of the most important symptoms, even though it is usually self-limiting without any permanent organ damage. Sickle cell anemia, high hematocrit and low fetal Hb are often associated with the occurrence of acute pain;
- Infection: sickle-cell disease may result in impaired spleen function, dysfunction of the complement system, and tissue ischemia, that imply an increase in infection rate of patients;
- Neurological complications: stroke in children is often caused by sickle-cell anemia, where vasculopathies affect the distal internal carotid and middle cerebral arteries. Silent infarcts are also noticed and are related to neurocognitive problems;
- Acute chest syndrome: it is a pneumonia-like disease that constitutes one main cause of morbidity of sickle-cell patients, characterized by pulmonary infiltrates on chest X-rays [15], and it is the result of vaso-occlusion and infection of the vasculature together;
- Pulmonary hypertension (PH): PH is a pathological condition to which sickle-cell disease leads, and it is highly related with patients' death;
- Heart disease: diastolic dysfunction is a frequent complication that affects about the 13% of adults with the pathology [12];
- Renal complications: HbS polymerization is very likely to be noticed in the renal medulla, where oxygen partial pressure and pH is low and osmolarity is high. These environmental characteristics easily lead to erythrocytes dehydration. Vaso-occlusion can also be noticed and renal infarction is its direct consequence.

1.2.1 Pulmonary Hypertension

PH is a pathological condition, where mean pulmonary artery pressure (mPap), a measure provided by right heart catheterization, reaches values higher than 25 mm Hg at rest, [16]: its value is estimated to be related to pulmonary vascular resistance (PVR) and right atrial pressure (RAP), as follows [17]:

Equation 1-mPap as a function of PVR and RAP

$$mPap = 4 * PVR^2 + RAP \qquad [mmHg]$$

where:

$$PVR = \frac{TRV}{TVI_{RVOT}} * 10 + 0.16$$

with TRV = tricuspid regurgitation peak velocity and TVI_{RVOT} = time-velocity integral right ventricular outflow tract. It is evident from Equation 1, how in the pulmonary artery, an increased pulmonary vascular resistance will lead to a higher pressure. This feature triggers the disease progression, due to the effort of the organism to restore homeostasis. Endothelial cells are one of the components of the arterial wall and their function involves the chemical signaling that regulate vasodilation and vasoconstriction: shear stresses are sensed by endothelial cells, which release chemicals like NO and endothelin-1, sensed by smooth muscle cells, that in turn are responsible for dilation or constriction. Presence of non-physiological shear stresses leads to intimal hyperplasia and impaired endothelium, which has been noticed in PH patients. The increased pulmonary arterial pressure is the starting point of the pulmonary hypertension evolution (Figure 1): luminal pressure and radius increase are the direct consequences of it. In turn, vessel wall thickness decreases and axial and circumferential stresses increase. The vascular system responds to this via remodeling in terms of wall compliance and thickness: vascular compliance decreases

and thickness increases. Increase in right-ventricle afterload and ventricle-vascular decoupling are the outcome of this process; a higher pulse pressure is noticed too in PH cases [18].

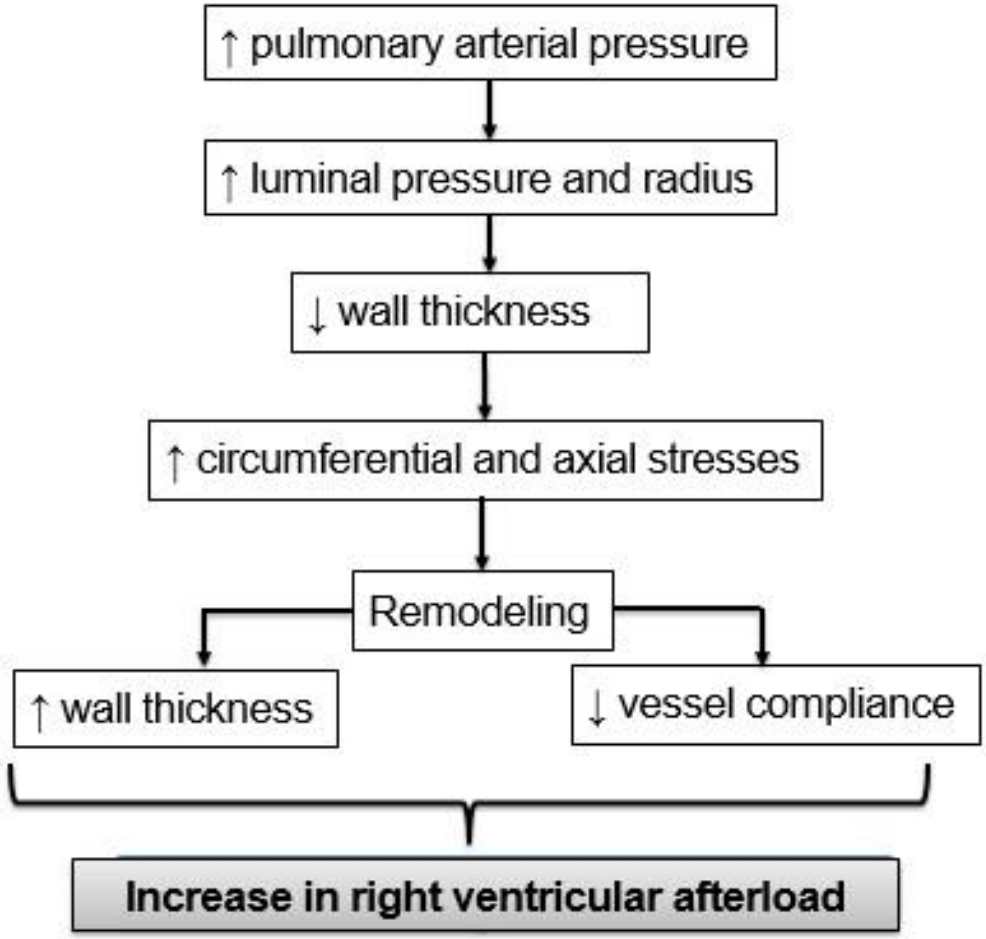

Figure 1-Pulmonary Hypertension disease progression

It is now evident how structural and mechanical changes, such as narrowing and stiffening, of the pulmonary vasculature are related to an increase in right ventricular (RV) afterload; arterial narrowing contributes to an increase in PVR, while arterial stiffening contributes directly to RV afterload.

For a better understanding of the various types of PH, in TABLE 2 is reported the classification made by the World Health Organization System (WHO).

TABLE 2- WHO CLASSIFICATION OF PULMONARY HYPERTENSION [19]

Group	Name	Details
Group 1	Pulmonary Arterial Hypertension (PAH)	Caused by precapillary PH due to an obstruction of the blood flow near the lungs capillary bed, that implies an increased PVR
Group 2	PH owing to left-heart disease	Left-sided heart pathological conditions could lead to a higher left arterial pressure, that implies an increase of PAP. PVR normal or near normal
Group 3	PH owing to lung diseases and/or hypoxia	Caused by alveolar hypoxia, implied by lung disease
Group 4	Chronic Thromboembolic PH	Result of the chronic pulmonary emboli with consequent secondary fibrotic remodeling
Group 5	PH with unclear or multifactorial etiologies	

Pulmonary arterial hypertension (PAH - Group 1 within WHO clinical classification system - TABLE 2) refers to a condition of PH disease where, from the hemodynamic point of view, pre-capillary PH is present: in this case, the end-expiratory pulmonary artery wedge pressure (PAWP) value is 15 mm Hg and PVR is measured to be higher than 3 Wood units. PAH affects small pulmonary arteries, consequently leading to proliferation of smooth muscle and tunica intima, and in-situ thrombosis: as an outcome, vessels narrow, leading ultimately to a damage of the vessels and an increment of pulmonary vascular resistance; this process implies an increase of the afterload on the right heart. Therefore, the right ventricle needs to rise its pumping effort and, progressively, this can lead to the failure of the right side of the cardiac muscle. In PAH, one can notice vasoconstriction, vessels remodeling, and thrombosis, that are the main causes of the higher pulmonary vascular resistance, and all layers of the vessels walls are modified due to vascular

remodeling. Some histological evidences have shown, in fact, intimal fibrosis, increased medial and adventitia thickness, and collagen accumulation [20]. From a cellular prospective, the following changes are involved [21]:

- Smooth muscle cells (SMC) and fibroblast: in PAH remodeling, the terminal part of SMCs extends into small, nonmuscular, pulmonary arteries within the respiratory acinus. The trigger of this process is yet to be determined. Moreover, in severe PH, between the internal elastic lamina and the endothelium, neointima is formed, namely a layer of myofibroblast and extracellular matrix. Neo-vascularization of vasa vasorum has also been shown to accompany vessel wall thickening, primarily in adventitia;
- Endothelial cells: endothelial cell proliferation in a disorganized way is a common phenomenon in PAH and it leads to the formation of plexiform lesions. Hypoxia, shear stress and inflammation are assumed to be some of the possible causes of this proliferation;
- Inflammatory cells: inflammatory mechanism is involved in some cases of PAH and it has been shown to take an important part in the overall process, even if further analysis is necessary to understand its role;
- Platelets and thrombosis: abnormalities in the clotting cascade and in the platelets action could be trigger for in situ thrombosis. In PAH, continuous intravascular coagulation, and an alteration of procoagulant activity and fibrynolitic function have been shown.

1.2.1.1 Diagnosis and Treatment

Although echocardiography has been shown to be the main non-invasive technique to assess the possibility of PH, it is still mandatory the use of right heart catheterization (RHC) to establish the diagnosis [19]. Echocardiography provides feasible measurement of pulmonary artery pressure,

but getting early PH diagnostic and screening information is intrinsically operator-limited [22]. Transthoracic echocardiography can assess peaks of the systolic pressure in the pulmonary artery and get information on how the right ventricle works; Doppler echocardiography gives a measure of blood flow and pressure gradients between the chambers. As reported above, RHC is the only established technique for assessing the presence of PH, since it directly provides pulmonary pressure and cardiac function measurements [23]. RHC has the big issue of being invasive: it consists in the insertion of a thin, flexible catheter in the groin or neck, that is guided by the doctor to the right part of the cardiac muscle and the pulmonary arteries, where measurements are done. Infections, bleeding complications, thrombosis, hemorrhages, and artery injuries are some of the risks linked to this technique. Other than RHC and transthoracic echocardiography, the 6-minute walk test (6MWT) is a widely-used method to have information on how the disease is progressing and on how the patient is responding to treatment. It involves the measurement of the distance that a patient is able to cover walking on a flat, hard, indoor floor. With this test, one is able to obtain information on functional performance during a physical activity comparable to the daily one [24]. As far as PH treatments are concerned, the main traditional focus was on vasodilator therapies, such as adenosine, epoprostenol, and NO. Currently, three types of agents are being used in the treatment of PH:

- Prostanoids: epoprostenol, treprostinil and iloprost are the approved drugs of this category, that have shown to reduce symptoms, and to cause improvements in hemodynamics and quality of life. They overcome the deficiency in prostacyclin I2, a molecule involved in platelet inhibition and vasodilation;
- Phospodiesterase 5 inhibitors (PDE-5): sildenafil and tadalafil inhibits the hydrolysis of cyclic Guanylyl Monophosphate (cGMP), which is part of the process that leads to

vasodilation. Improved hemodynamics and increased distance in the 6MWT have been shown as a response to this treatment;

- Endothelin-1 receptor antagonist: endothelin-1 is a molecule that once bond to its receptor strongly leads to vasocontriction. Bosentan and Ambrisentan are endothelin receptor antagonist, which blocking endothelin action, promote vasodilation.

1.3 Background and Motivation

Computational Fluid Dynamics (CFD) is progressively becoming an important instrument for getting information about the cardiovascular system; assessing progression of the disease, treatment response, and surgical planning are some of the possible applications of such analysis. With the current knowledge from research, multiple systems at once can be simulated with CFD. This level of complexity goes sometimes beyond what is experimentally measurable, and that is another advantage of this technique. Arteries, veins, and capillaries that constitute the cardiovascular system are arranged in complex branching networks, and models to simulate them have to deal with this geometry. The current state of the art reports research on network models starting from the late Fifties, and in more than half a century this field of study improved a lot. Womersley [25] laid the foundations of this field in 1957, inquiring the pulsatile flow in arteries. Starting from Womersley's study, the research on this topic approaches the problem in two different ways. A first approach is the time-domain one, in which continuity and momentum equations are taken into consideration. These equations need the specification of further relationships to be solved, which are given by a pressure-area and a shear stress relationship. As said before, the solution is computed in the time domain by means of proper numerical methods, and the propagation of either pressure and flow waves along the arteries can be studied. The advantage of this method is that it includes non-linearities, such as convective terms of the

Navier-Stokes equation and pressure-area relationship. A second approach to such a problem takes advantage of an electrical analogue, the so-called transmission line, which is carried out in the frequency domain. This approach allows to inquire how pressure and flow harmonics propagate in each segment of the branching network [26]. Both approaches to the problem relies on the choice of proper boundary conditions, one at the inlet and one at the outlet. The inflow boundary condition is usually given by pressure or flow waveform measured at the inlet of the arterial network. As far as the outflow boundary condition is concerned, terminal impedance must be known and different models can be used:

- Zero traction: this approach consists in considering the pressure at each outlet to be a constant value;
- Pure resistance: each terminal segment is considered to be connected to a simple resistor. This choice has the disadvantage of not taking into account the compliance nature of distal vessels and of maintaining pressure and flow in phase;
- Windkessel model: distal arteries can be represented with an electrical analogue that accounts both for resistance and compliance: typically, an RCR circuit is considered. Higher complexity can be obtained adding and inductance, with the so-called four elements Windkessel model.
- Structured tree: this model consists in modelling vasculature distal to a truncation point with a structured tree.

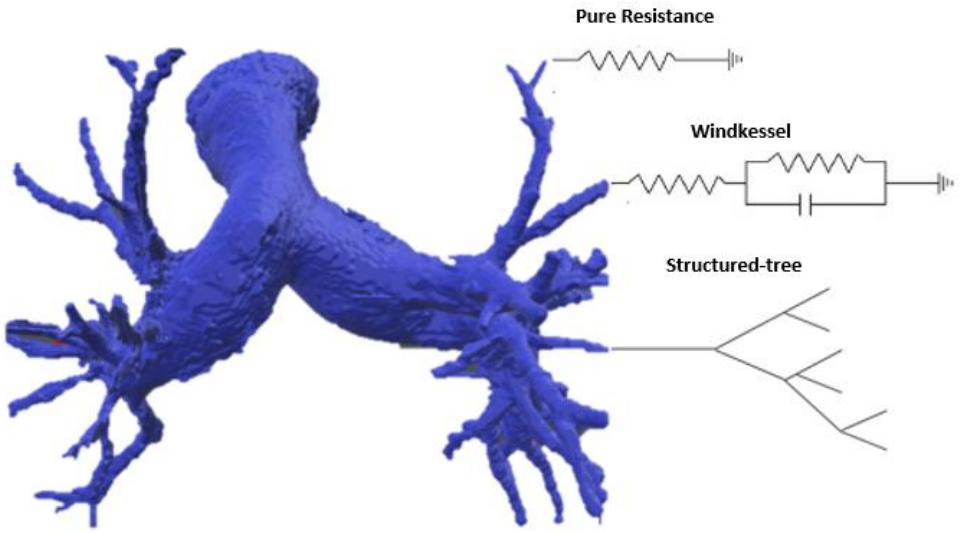

Figure 2-Outflow Boundary Condition

One of the first studies on this topic was carried out by Attinger in 1963, who focused on how the pressure pulse was transmitted in the pulmonary arteries of living dogs, and on the superimposition of transmitted and reflected waves [27]. In 1966, Wiener et al. developed an analytical model for the wave propagation in the pulmonary circulation, and noticed that the shape of pressure or flow wave mainly changed due to reflection phenomena [1]. Pollack et al. [28], studied the pulmonary arterial tree with an electrical analogue in 1968, inquiring also the effect of vasoconstriction. Milnor et al. [29] measured blood flow in the pulmonary arteries of both healthy and diseased (pulmonary hypertension and mitral stenosis) patients. In 1980, Avolio [30] built a model of the systemic arteries, considering 128 segments in a branching structure and taking into account viscoelasticity. Olufsen et al. [2], in 2000, inquired flow in systemic arteries with a one-dimensional time-domain model which introduced for the first time the structured tree outflow boundary condition. In 2007, Spilker [31] developed a patient-specific model of pulmonary arteries which relied on morphometry-based impedance boundary conditions, characterized also by a tuning analysis to obtain physiological pressure and flow in the distal

vasculature. In 2014, Qureshi et al. coupled arterial and venous circulation in a time-domain model [32]. The current work focuses on the pulmonary circulation and on the construction of an analytical model in the frequency domain that can give information on pressure and flow along the vessel network. This model is also used to simulate sickle cell disease and its progression, which leads to pulmonary hypertension. This pathology, as explained before, modifies from a structural and a mechanical point of view vasculature and this affects the propagation of pressure and flow waves. A model able to give reliable information on pressure and flow throughout the pulmonary circulation in a short time can be of great clinical interest. Application of such a model range from monitoring disease progression and/or response to treatment, to planning intervention and integrating experimental data for diagnostic purposes. This preliminary study tries to lay the foundation for obtaining a tool with this potential. Computations are performed in the frequency domain and the approach chosen considers the structured tree as an outflow boundary condition; a finite element model has also been used for the validation of the analytical model.

1.4 Objectives

The current work develops an analytical model with the goal of simulating the propagation of pressure and flow waves along the pulmonary circulation in the frequency domain. The pulmonary circulation is outlined as one-dimensional branching waveguide and each blood vessels is modeled as a transmission line. The first objective of this work is the validation of the developed analytical model. A finite element (FE) simulation is set up, and the results is compared with the analytical result. The validation of the analytical model relis on the agreement between the results of the two models.

Pressure and flow within the pulmonary circulation are pulse waves generated by the contraction of the right ventricle. It is of particular interest in this work to inquire whether a model in the frequency domain gives all the information necessary to reconstruct the arterial pulse waveform in the time domain. In the frequency domain, the spectrum of a pulse wave is characterized by different peaks at different frequencies, each one representing one harmonic. The superposition principle is used to sum up the different analytical solutions for the different harmonics, thus to simulate the pulse wave in the frequency domain. Performing Fourier transform, the pulse waveform in the time domain is consequently obtained.

Sickle cell disease and pulmonary hypertension is also taken into consideration in the current work to analyze a possible application of the analytical model. As explained in Section 1.2.1, sickle cell disease causes vaso-occlusion in the microcirculation, whereas pulmonary hypertension, causes mechanical and structural changes in the pulmonary arteries, which affect wave propagation. The analytical model is used to analyze the effect of sickle cell disease and pulmonary hypertension on wave propagation.

The current work is a preliminary evaluation of the potential of a frequency-domain analytical model and of its possible application. The long-term objective of this work is obtaining a reliable, versatile, time-saving tool, able to obtain useful pieces of information, in a clinical perspective, like patient-specific prediction of the pressure along the pulmonary circulation. Such a tool could give to the clinicians, for example, the possibility of a first approximation of the response to a treatment, improving the planning process.

CHAPTER 2

THEORY

In order to fulfill the objectives reported in Section 1.3, an analytical model which takes into consideration the entire pulmonary circulation is needed.

The model consists of two fundamental parts, that can be modified to fit the case of study in the best way. The first one is the mathematical description of the acoustic properties of an individual vascular segment; the approach to fully describe the behavior of the single element consists in coupling the movement of the fluid with the motion of the walls of the waveguide in which the fluid is contained. Secondly, a geometry resembling the branching of the pulmonary vasculature is required, which usually is generated with bifurcation algorithm. The combination of the single element equation and the selected geometry allows the complete analysis of the system, thus the wave propagation can be studied.

2.1 Wave propagation

As reported in Paragraph 1.1, the cardiovascular system is characterized by pulsatile flow that, related to the properties of vessels and blood, has as a major effect the attenuation of the pulse wave during its travel. For having a better understanding of the phenomenon, one can start from the simplest case of an infinitely long, cylindrical, straight tube made of an elastic material, which contains an incompressible non-viscous fluid. If a disturbance is applied at one end of the tube, it will be propagated as a wave along the tube at a certain velocity.

This behavior can be mathematically expressed as a wave equation, which is, in terms of pressure:

Equation 2-Wave equation in terms of pressure

$$\frac{\partial^2 p}{\partial x^2} - \frac{1}{c^2}\frac{\partial^2 \mathrm{p}}{\partial t^2} = 0$$

Where:

- p is the pressure;
- c is the wave velocity.

The solution of Equation 2 is of the following form:

Equation 3-Solution of the 1-D wave equation

$$p(x,t) = f(x - ct)$$

Where the term $x - ct$ represents a wave travelling in the direction of the positive *x-axis*; all the way around, a wave propagating in the negative *x* direction, will be referred to as $p(x,t) = g(x + ct)$, as it can be noticed in Figure 3.

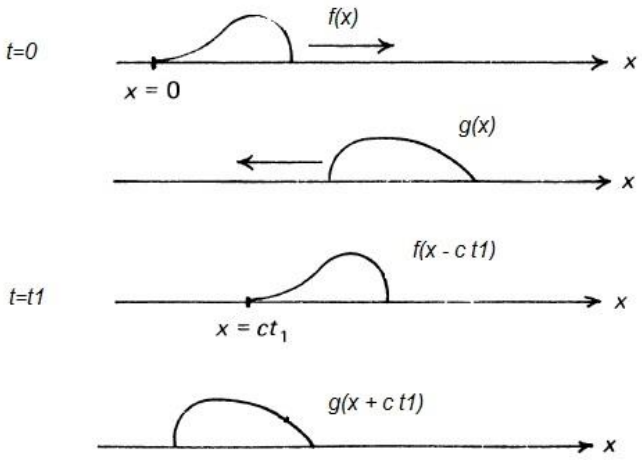

Figure 3-Wave propagating to the right and to the left

If some frictional losses are obtained, the wave equation can be modified to take into account even the related damping. The general form of the damped wave equation is the following:

Equation 4-General damped wave equation

$$\frac{\partial^2 p}{\partial x^2} = \frac{1}{c^2}\left(\frac{\partial^2 p}{\partial t^2} + K\frac{\partial p}{\partial t}\right)$$

where $K\frac{\partial p}{\partial t}$ is the damping term representing the frictional losses, that result in an exponential decay of the wave propagating away from the source. Assuming for example a sinusoidal disturbance in the positive *x* direction, the damped wave equation is solved by an exponential equation, such as:

Equation 5-Solution of the damped wave equation in response to a sinusoidal disturbance

$$p(x,t) = p_0 e^{i(\omega t - \gamma x)}$$

Where:

- $\gamma = \alpha + i\beta$, is the propagation constant, with α that is the damping constant (attenuation per unit length) and β that is the phase shift per unit length;
- ω=circular frequency, [rad/sec].

The phase velocity is defined as the velocity of travel of a simple harmonic perturbation, and can be mathematically expressed as:

Equation 6-Phase velocity

$$v_p = \frac{\Delta l}{\Delta \theta}\omega = \frac{\Delta l}{\Delta \theta}2\pi f = \frac{\omega}{\beta} = \lambda f$$

Where:

- v_p is the phase velocity;
- Δl is the distance over which the phase velocity is measured;
- $\Delta\theta$ is the difference in phase angle between the two measurements;
- λ is the wavelength;
- f is the frequency.

Moens-Kortweg equation for phase velocity holds for a simple elastic case:

Equation 7-Moens-Kortweg equation

$$v_p^2 = \frac{Eh}{2\rho r}$$

with:

- E = vessel wall Young's modulus;
- ρ = blood density;
- r = vessel radius;
- h = vessel wall thickness.

Phase velocity determination provides a versatile and simple tool to get theoretically the elastic properties of a blood vessel, which diagnostic application has been inquired in the past years[34],[35]; differently from the phase velocity, one can deal with the concept of group velocity, that is defined as the velocity at which the compound wave travels, instead of the energy.

Equation 8-Group velocity

$$v_g = \frac{\partial\omega}{\partial\beta}$$

Other than the propagation constant, the behavior of a single segment of tube is to be related to the characteristic impedance too, which represents the relationship between the pressure and the flow at the entrance of an infinitely long tube, without considering any reflection. It can be expressed as:

Equation 9-Characteristic impedance

$$Z = \frac{p}{q}$$

This parameter is a complex value, characterized by both magnitude and phase, and in the case of a blood vessel, it considers the viscoelastic and inertial effect related to it. Moving to the end of the segment, one can define another parameter, the load impedance, which as the characteristic impedance, is pressure-to-flow ratio, but at the end of the tube. Considering two consecutive segments, if their properties are different, namely the load impedance of the first is different from the input impedance of the last, the wave propagation is affected. The occurring impedance mismatch implies the generation of a reflected waves, travelling backwards the segment: the steady state wave in the segment will be given by the superposition of the two.

2.1.1 Wave reflection at a bifurcating point

An interesting case of impedance mismatch to be analyzed is a bifurcation point, namely a parent tube that branches into two daughter tubes, as shown in Figure 4.

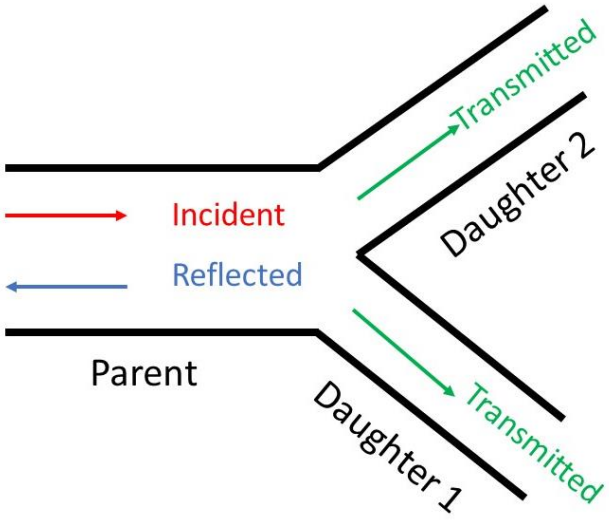

Figure 4-Bifurcating pattern of a blood vessel

A wave travelling down the parent tube, that reaches the junction, is influenced by this conformation, and will be modified, as explained by Fung[7]. At the junction, either the reflection or the transmission phenomenon must be taken into consideration: a part of the incident wave, in fact, will be reflected, and the remaining will be transmitted down to the daughters. At the end of the parent tube, so at the bifurcation point, the conditions that must be imposed are the following:

a. Single value of pressure;
b. Continuity of flow.

These conditions can be summarized with the following equations:

Equation 10-Condition of (a) pressure and (b) volume-flow rate at the bifurcation point

$$\begin{cases} p_I + p_R = p_{T1} = p_{T2} & (a) \\ q_I - q_R = q_{T1} + q_{T2} & (b) \end{cases}$$

Where the subscript *I* stands for *incident*, *R* for *reflected*, *T* for *transmitted*. Reminding the relationship between pressure and volume-flow rate, reported in Equation 9, one can rewrite Equation 10b as follows:

Equation 11

$$\frac{p_I - p_R}{Z_0} = \frac{p_{T1}}{Z_1} + \frac{p_{T2}}{Z_2}$$

Replacing Equation 10b with Equation 11, and solving the system for the pressures, one obtains:

Equation 12-(a) Reflection coefficient, (b) Transmission coefficient

$$\begin{cases} \dfrac{p_R}{p_I} = \dfrac{\dfrac{1}{Z_0} - \left(\dfrac{1}{Z_1} + \dfrac{1}{Z_2}\right)}{\dfrac{1}{Z_0} + \left(\dfrac{1}{Z_1} + \dfrac{1}{Z_2}\right)} = \mathcal{R} & (a) \\ \dfrac{p_{T1}}{p_I} = \dfrac{p_{T2}}{p_I} = \dfrac{\dfrac{2}{Z_0}}{\dfrac{1}{Z_0} + \left(\dfrac{1}{Z_1} + \dfrac{1}{Z_2}\right)} = \mathcal{T} & (b) \end{cases}$$

Equation 12a and b give an idea of the amplitude of both the reflected and the transmitted waves: the reflected wave will be $\mathcal{R}$ times the incident wave, while the transmitted one will be $\mathcal{T}$ times the incident one. Starting from the definition of reflection and transmission coefficient, incident, reflected and transmitted waves can be easily expressed. Let the incident pressure wave be:

Equation 13-Incident wave

$$p_I = p_0 f\left(t - \frac{x}{c_0}\right)$$

If the bifurcation is situated at $x = 0$, the incident wave at the junction will be:

Equation 14-Incident wave at the junction

$$p_I = p_0 f(t)$$

Consequently, reflected and transmitted waves turn out to be:

Equation 15-(a) Reflected wave, (b) and (c) transmitted waves

$$\begin{cases} p_R = \mathcal{R} p_0 f\left(t + \dfrac{x}{c_0}\right) & (a) \\ p_{T1} = \mathcal{T} p_0 f\left(t + \dfrac{x}{c_1}\right) & (b) \\ p_{T2} = \mathcal{T} p_0 f\left(t + \dfrac{x}{c_2}\right) & (c) \end{cases}$$

Where c_0, c_1 and c_2 are the wave velocities in the corresponding tubes.

2.1.2 Multiple reflection

The pulmonary circulation is a highly complex system, characterized by multiple junctions and for being fully described in terms of pressure and flow waves multiple reflection at different junctions must be taken into consideration. Referring to Figure 5, one can start analyzing a wave travelling from A to B. Once the wave reaches the junction in B is partially reflected and partially transmitted: the reflected wave will go back towards A, while the transmitted waves will travel towards C and D. Taking into consideration the tube 1, one can notice that the transmitted wave from B will travel towards C and once at the junction will be both reflected and transmitted. When the reflected wave in C reaches back B, will be further reflected towards C and transmitted towards A and D and so on.

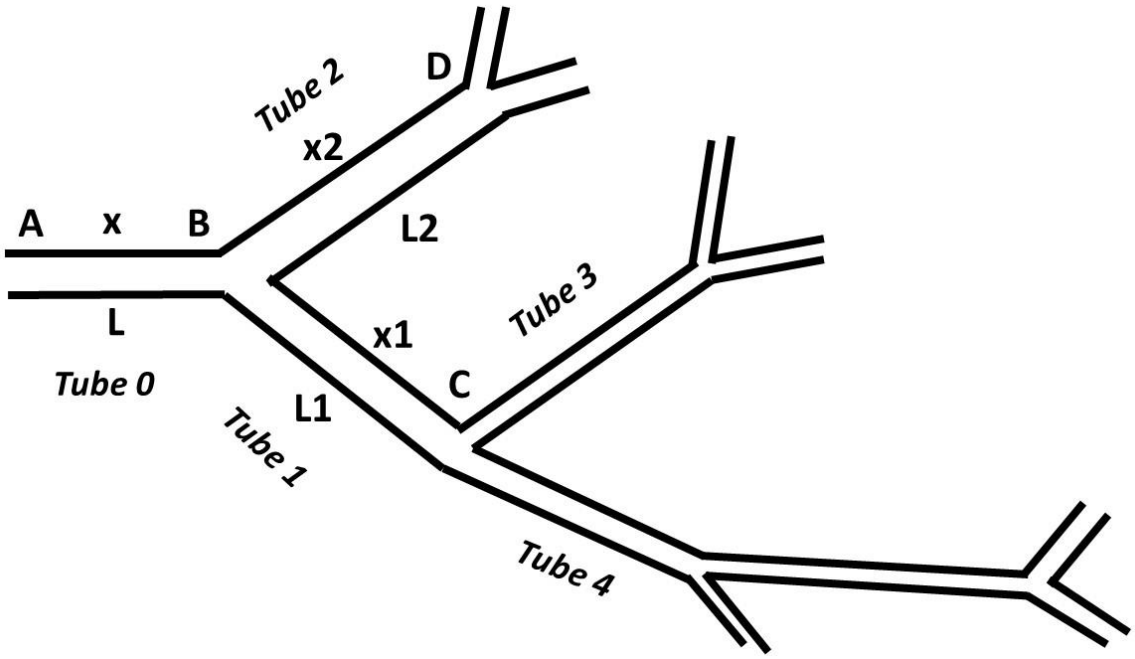

Figure 5-Sketch of multiple junctions present in the pulmonary vasculature (x=coordinate along the segment, L=length of the segment)

The process continues and in each segment the waves both bounce back and forth and are transmitted in adjacent segments: in each segment the pressure perturbation is the sum of all these waves. It is worthy noticing that multiple reflection is a major phenomenon affecting blood flow, that in turn influences pressure as well. Given that at any point the pressure and flow are affected both by newly arrived waves and retarded reflected waves, it is evident the frequency dependence of the pressure-flow relationship. If one wants to couple the pulmonary circulation with the heart, the input impedance at the pulmonary valve must be known. To obtain it, one can combine the solution of the single segment with the geometrical pattern of the bifurcation. Considering the simple case without frictional losses, the pressure wave in the tube 0 from A to B be:

Equation 16-Pressure wave in tube 0

$$p = p_I e^{i\omega\left(t-\frac{x}{c_0}\right)}$$

This wave at the point B, namely when x = L, will be:

Equation 17-Pressure wave in x=L

$$p = p_I e^{i\omega\left(t-\frac{L}{c_0}\right)}$$

In point B, this wave will be either reflected or transmitted; combining Equation 17 with Equation 15, a, b, and c, it comes out:

Equation 18-(a) Reflected wave, (b), (c) transmitted waves

$$\begin{cases} p_{RBA} = p_R e^{i\omega\left[t-\frac{L}{c_0}-\frac{(L-x)}{c_0}\right]} & \text{(a)} \\ p_{TC} = p_{T1} e^{i\omega\left[t-\frac{L}{c_0}+\frac{x_1}{c_1}\right]} & (b) \\ p_{TD} = p_{T2} e^{i\omega\left[t-\frac{L}{c_0}+\frac{x_2}{c_2}\right]} & (c) \end{cases}$$

The pressures in the point B, where x = L, $x_1 = x_2 = 0$, are:

Equation 19-(a) Reflected wave, (b), (c) transmitted waves in B

$$\begin{cases} p_{RBA} = p_R e^{i\omega\left[t-\frac{L}{c_0}\right]} & \text{(a)} \\ p_{TC} = p_{T1} e^{i\omega\left[t-\frac{L}{c_0}\right]} & (b) \\ p_{TD} = p_{T2} e^{i\omega\left[t-\frac{L}{c_0}\right]} & (c) \end{cases}$$

Applying the conditions on pressure and flow reported in Equation 10a and b, and cancelling out the term $e^{i\omega\left[t-\frac{L}{c_0}\right]}$, one obtains:

Equation 20-Condition on (a) pressure and (b) flow at the junction in point B

$$\begin{cases} p_I + p_R = p_{T1} = p_{T2} & (a) \\ \frac{p_I}{Z_0} - \frac{p_R}{Z_0} = \frac{p_{T1}}{Z_1} + \frac{p_{T2}}{Z_2} & (b) \end{cases}$$

By solving this system for the pressures, it comes out:

Equation 21-Expression for the effective (a) reflection coefficient, (b) transmission coefficient

$$\begin{cases} \dfrac{p_R}{p_I} = \dfrac{\dfrac{1}{Z_0} - \left(\dfrac{1}{Z_1} + \dfrac{1}{Z_2}\right)}{\dfrac{1}{Z_0} + \left(\dfrac{1}{Z_1} + \dfrac{1}{Z_2}\right)} = \mathcal{R} & (a) \\ \dfrac{p_{T1}}{p_I} = \dfrac{p_{T2}}{p_I} = \dfrac{\dfrac{2}{Z_0}}{\dfrac{1}{Z_0} + \left(\dfrac{1}{Z_1} + \dfrac{1}{Z_2}\right)} = \mathcal{T} & (b) \end{cases}$$

At point A, namely where $x = 0$, assuming no further reflection for the reflected wave, pressure and the flow will be:

Equation 22-Resultant (a) pressure and (b) flow waves in point A

$$\begin{cases} p_A = p_I e^{i\omega t} + p_R e^{i\omega\left(t - \frac{2L}{c_0}\right)} = p_I e^{i\omega t}\left(1 + \mathcal{R}\ e^{-i\omega\frac{2L}{c_0}}\right) & (a) \\ q_A = \dfrac{p_{IA} + p_{RA}}{Z_0} = \dfrac{p_I e^{i\omega t}}{Z_0}\left(1 - \mathcal{R}\ e^{-i\omega\frac{2L}{c_0}}\right) & (b) \end{cases}$$

One can now calculate the ratio between p_A and q_A, which is the input impedance at A:

Equation 23-Input impedance at point A

$$Z_{in\_A} = \frac{p_A}{q_A} = Z_0 \frac{1 + \mathcal{R}\ e^{-i\omega\frac{2L}{c_0}}}{1 - \mathcal{R}\ e^{-i\omega\frac{2L}{c_0}}}$$

Replacing $\mathcal{R}$ with the expression reported in Equation 21a, multiplying both numerator and denominator by $\frac{1}{Z_0} + \left(\frac{1}{Z_1} + \frac{1}{Z_2}\right) e^{-i\omega\frac{L}{c_0}}$, and recalling the relations:

$$\begin{cases} \dfrac{e^{i\alpha} + e^{-i\alpha}}{2} = cos\,\alpha \\ \dfrac{e^{i\alpha} - e^{-i\alpha}}{2} = i\ sen\,\alpha \end{cases}$$

the following fundamental result is obtained:

Equation 24-Imput impedance at point A

$$\frac{1}{Z_{in\_A}} = \frac{1}{Z_0}\frac{\left(\frac{1}{Z_1}+\frac{1}{Z_2}\right)+i\frac{1}{Z_0}\tan\left(\omega\frac{L}{c_0}\right)}{\frac{1}{Z_0}+i\left(\frac{1}{Z_1}+\frac{1}{Z_2}\right)\tan\left(\omega\frac{L}{c_0}\right)}$$

The repeated application of Equation 24 allows to obtain at each point the effective impedance, namely the relationship between the pressure oscillation and the flow, starting from their distal values. This result for the simple case can be generalized even for the propagation of a wave in a dispersive medium, thus considering the damping, and can be extended to the whole tree-like structure of the pulmonary circulation. Starting from a damped wave of the form:

Equation 25- Solution of damped wave equation

$$p(x,t) = p_0 e^{i(\omega t-\gamma x)}$$

One obtains:

Equation 26-Input impedance with a damped wave

$$\begin{cases} Z_{in} = Z_0\dfrac{1+\mathcal{R}\ e^{-i2\gamma L}}{1-\mathcal{R}\ e^{-i2\gamma L}} \\ \dfrac{1}{Z_{in}} = \dfrac{1}{Z_0}\dfrac{\left(\frac{1}{Z_1}+\frac{1}{Z_2}\right)+i\frac{1}{Z_0}\tan(\gamma L)}{\frac{1}{Z_0}+i\left(\frac{1}{Z_1}+\frac{1}{Z_2}\right)\tan(\gamma L)} \end{cases}$$

CHAPTER 3

ANALYTICAL MODEL

The analytical model to approach this problem can be divided in two steps:

1. Definition of proper governing equations for the single segment of vasculature;
2. Integration of these equations in the complex geometry.

The solution of such a problem relies on the choice of proper boundary condition, since differential equation are involved. In this case, the impedance at the distal end, considered to correspond to the pulmonary capillaries, is assumed to be known, as the pressure at the top of the main pulmonary artery is as well.

Two main parts constitutes the current model: large arteries and small arteries. In the large arteries, values for blood flow and pressure are computed pointwise along the branching network. As far as the small arteries are concerned, they are represented as structured asymmetrically bifurcating tree, attached at each terminal of the large arteries. These two parts differ in terms of governing equations, boundary conditions and geometry.

3.1 Large arteries

In this work, the model proposed by Wiener et al. [1] was followed in terms of the description of the single vascular segment of the large arteries. The individual segment is described as a uniform elastic thin-walled cylinder with a negligible mass, filled with a Newtonian and incompressible fluid, assuming axisymmetric motion.

Considering the fluid motion first and starting from Navier-Stokes equation for this case, one is able to such equations with the following additional assumptions:

a. The radius of the tube is large compared to its radial displacement;
b. The tube radius is smaller than the wavelength;
c. The mean flow velocity is small compared to the wave velocity;
d. The attenuation per wavelength is small.

The linearized equation for the fluid motion turned out to be the following:

Equation 27-Fluid motion: linearized Navier-Stokes equation

$$-\frac{\partial p}{\partial x} = L\frac{\partial q}{\partial t} + Rq$$

Where:

- p = pressure, [dyn/cm^2];
- q = volume-flow rate, [cm^3/sec];
- L = fluid inertia per unit length, [dyn sec^2/cm^5] per cm;
- R = fluid resistance per unit length, [dyn sec^2/cm^5] per cm.

Fluid inertia and resistance are defined as follows:

Equation 28-Fluid resistance

$$R = \frac{\rho\omega}{\pi r^2 M}\sin\theta$$

Equation 29-Fluid Inertia

$$L = \frac{\rho}{\pi r^2 M}\cos\theta$$

Where M and θ represent respectively magnitude and phase of the following expression:

Equation 30 - Definition of M and θ

$$Me^{i\theta} = 1 - \frac{2J_1\left(\alpha i^{\frac{3}{2}}\right)}{\alpha i^{\frac{3}{2}} J_0\left(\alpha i^{\frac{3}{2}}\right)}$$

With:

- J_0, J_1 = Bessel function of order 0,1;
- $\alpha = r\sqrt{\frac{\rho\omega}{\mu}}$ = Womersley number.

As far as the wall motion is concerned, Wiener et al. related first the pressure at the wall with the radial displacement of the tube (Equation 31a); then, this equation was coupled with the one of the fluid motion, imposing that at the wall the radial velocity of fluid v_r and of wall $\frac{\partial u_r}{\partial t}$ are equal, and obtaining a continuity equation for the blood (Equation 31b):

Equation 31- Wall motion: (a) Pressure at the wall as a function of the radial displacement; (b) equation of continuity for blood, integrated over cross-section area

$$\begin{cases} p = \dfrac{Eh}{1-\upsilon^2}\dfrac{u_r}{r_0} & (a) \\ \dfrac{\partial q}{\partial x} = -2\pi r_0 v_r & (b) \end{cases}$$

Where:

- E = Young's modulus, [dyn/cm^2];
- h = wall thickness, [cm];
- u_r= radial displacement of the wall, [cm];
- υ = Poisson's ratio for the wall, [-];

- r_0= vessel radius, [cm];
- v_r= radial velocity of the fluid, [cm/sec].

Combining Equation 31a and b, one obtains:

Equation 32-Wall motion: pressure-flow relationship

$$\frac{\partial q}{\partial x} = -C\frac{\partial p}{\partial t}$$

Where:

- $C = \frac{2(1-\upsilon^2)\pi {r_0}^2}{E}\frac{r_0}{h}$ = compliance per unit length, [cm^4/dyn].

From the combination of the fluid motion equation (Equation 27) and the wall motion equation (Equation 32), the damped wave equation is obtained, expressed either in terms of pressure or in terms of flow:

Equation 33-Damped wave equation in terms of pressure (a) and flow (b)

$$\begin{cases} L\frac{\partial^2 p}{\partial t^2} - \frac{1}{C}\frac{\partial^2 p}{\partial x^2} + R\frac{\partial p}{\partial t} = 0 & \text{(a)} \\ L\frac{\partial^2 q}{\partial t^2} - \frac{1}{C}\frac{\partial^2 q}{\partial x^2} + R\frac{\partial q}{\partial t} = 0 & \text{(b)} \end{cases}$$

Starting from the values of instantaneous pressure and instantaneous flow:

Equation 34-Instantaneous values of pressure (a) and flow (b)

$$\begin{cases} p = Re\{Pe^{i\omega t}\} & (a) \\ q = Re\{Qe^{i\omega t}\} & (b) \end{cases}$$

Where:

- ω=circular frequency, [rad/sec].

and plugging them into Equation 33, a or b, one may obtain, after a proper integration, a solution of the form of:

Equation 35-Form of the solution of Equation 33 in terms of (a) pressure and (b)flow (constants A and B are still to be determined)

$$\begin{cases} P = Ae^{-\gamma x} + Be^{\gamma x} & (a) \\ Q = \dfrac{1}{Z_0}(Ae^{-\gamma x} - Be^{\gamma x}) & (b) \end{cases}$$

Where:

- $\gamma = \sqrt{i\omega C(R + i\omega L)}$;
- $Z_0 = \sqrt{\frac{R+i\omega L}{i\omega C}}$ = characteristic impedance.

The solution of Equation 33 depends on the choice of proper boundary conditions, that are needed to find the integration constants A and B: in this case, the impedance at the distal terminal of the tube, Z_T, and the pressure at the inlet of the tube, P_{in}. The outflow boundary condition, namely the value of the impedance at each terminal of the large arteries, comes from the small arteries, as described by Olufsen et al. [2]. With simple assumption, the behavior of the small arteries is fully described and the root impedance can be found, which constitutes the outflow boundary impedance for large arteries. It is worth reminding that the characteristic impedance at any point, x, can be written as:

Equation 36-Characteristic impedance

$$Z = \frac{Pressure}{Volume\ flow\ rate}$$

With the application of the boundary value Z_T, the impedance at the proximal end, $Z_{in,}$ can be written as:

Equation 37-Expression of the proximal impedance Z_{in}

$$Z_{in} = Z_0 \frac{1 - \mathcal{R}e^{-2\gamma L}}{1 - \mathcal{R}e^{-2\gamma L}}$$

Where:

- L = length of the segment, [cm];
- $\mathcal{R} = \frac{Z_0 - Z_T}{Z_0 + Z_T}$ = reflection coefficient for flow at the distal tube.

With the mathematical steps shown in Paragraph 2.1.2, one can rewrite the input impedance as follows:

Equation 38-Input impedance

$$Z_{in} = \frac{Z_T + Z_0 tanh(\gamma L)}{1 + \frac{Z_T}{Z_0} tanh(\gamma L)}$$

Knowing the pressure P_{in} or the flow Q_{in} from the boundary conditions, the impedance Z_{in} obtained from Equation 37, one is able to find A and B and to rewrite Equation 35a and b, as follows:

Equation 39-Solution of Equation 33 in terms of (a) pressure and (b) flow

$$\begin{cases} P = P_{in}\left(\frac{Z_{in} + Z_0}{2Z_{in}} e^{-\gamma x} + \frac{Z_{in} - Z_0}{2Z_{in}} e^{\gamma x}\right) & (a) \\ Q = Q_{in}\left(\frac{Z_0 + Z_{in}}{2Z_0} e^{-\gamma x} + \frac{Z_0 - Z_{in}}{2Z_0} e^{\gamma x}\right) & (b) \end{cases}$$

The properties of an individual vascular segment of the large arteries are in this way fully described.

3.1.1 Geometry

The geometry of the large arteries was obtained from anatomical data. A set of de-identified human Computerized Tomography (CT), courtesy of Paras Parikh (AHA Award #14PRE20450163, "A geometric-based estimation of atrial wall stress for the prediction of remodeling in patients with atrial fibrillation.", 2014), has been used to obtain a fully characterized tree in terms of geometrical dimensions (radii, length, and thickness of each segment) and structure of the vessel network. Values of length and diameter have been computed from the CT images with the use of a Graphic User Interface (GUI) developed in MATLAB ("MATLAB R2016b, The MathWorks, Natick, 2016"). This tool was able to compute radius and length of each segment as distance between two points selected by the users, and to store the information in a matrix suitable for further analysis in MATLAB.

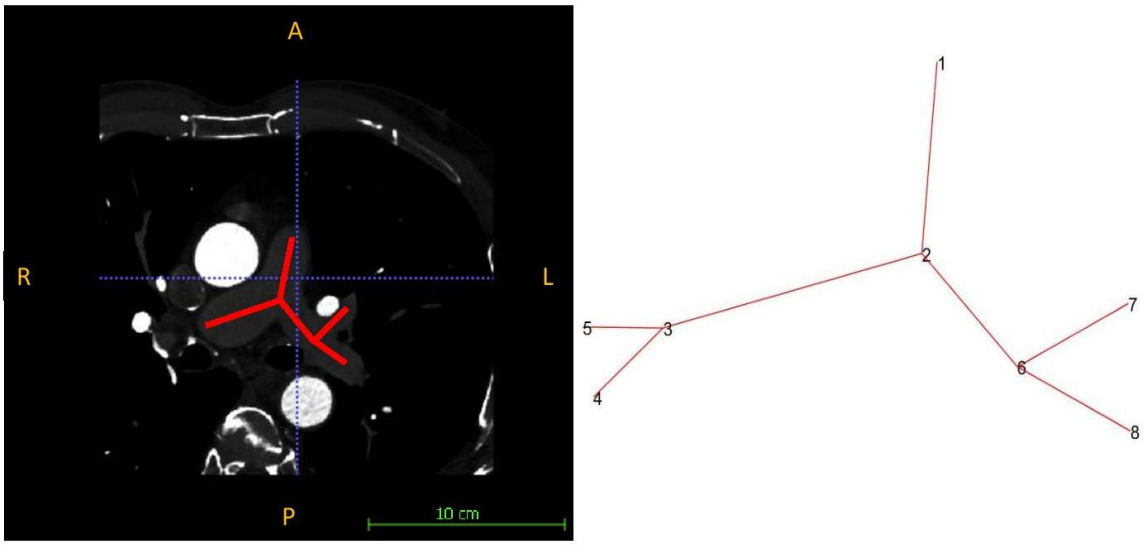

Figure 6 - Extrapolation of the one-dimensional geometry for large arteries from CT

Values of thickness was manually assigned considering a constant ratio between radius and thickness: thickness was, in fact, considered to be 30% of the radius. This geometry has been

truncated at a certain level of detail due to the high complexity of the tree and this is the reason why the tree needed to be completed by means of small arteries.

3.2 Small arteries

All the vasculature, distal to the end of large arteries, is represented by a structured tree; the data for the creation of small arteries tree comes from morphometric studies and the aim is to find its input impedance, that gives the outflow boundary condition needed. To accomplish this goal, the procedure consists in starting from the terminal segments, where a zero terminal impedance is considered as outflow boundary condition [2], and working recursively upstream. Small arteries input impedance is obtained from the following formula:

Equation 40 - Input impedance of the structured tree, resembling small arteries

$$Z(0,\omega) = \frac{i\, g^{-1} sin(\frac{\omega L}{c}) + Z(L,\omega) cos(\frac{\omega L}{c})}{cos\left(\frac{\omega L}{c}\right) + i\, g\, Z(L,\omega) sin(\frac{\omega L}{c})}$$

Where:

- $g = \sqrt{\frac{C\, A\, (1-F_{10})}{\rho}}$;
- $c = \sqrt{\frac{A\,(1-F_{10})}{C\rho}}$;
- $g = \sqrt{\frac{C\, A\, (1-F_{10})}{\rho}}$;
- $C = \frac{3Ar}{2Eh}$;
- $F_{10} = \frac{2J_1\left(\alpha i^{\frac{3}{2}}\right)}{\alpha i^{\frac{3}{2}} J_0\left(\alpha i^{\frac{3}{2}}\right)}$;
- $\alpha = r\sqrt{\frac{\rho\omega}{\mu}}$ = Womersley number.

3.2.1 Geometry

The geometry of the pulmonary arterial tree has been deeply investigated throughout the past and it has been described mostly with branching patterns. One of the main morphometric studies on the subject was proposed by Horsefield [36] in 1973, in which the description of the branching system, outlining the vascular tree followed the order grouping system proposed by Strahler [37], shown in Figure 7. This method consisted in assigning the order 1 to the most distal branches, in the case of the arterial tree considered to be the smallest noncapillary blood vessels, and proceeding backwards with a unitary increase of the order two branches meet: two branches of order 1 give rise to a branch of order 2, two branches of order 2 give rise to a branch of order 3, and so on; the meeting of two vessels of different order give rise to a branch of order equal to the larger one.

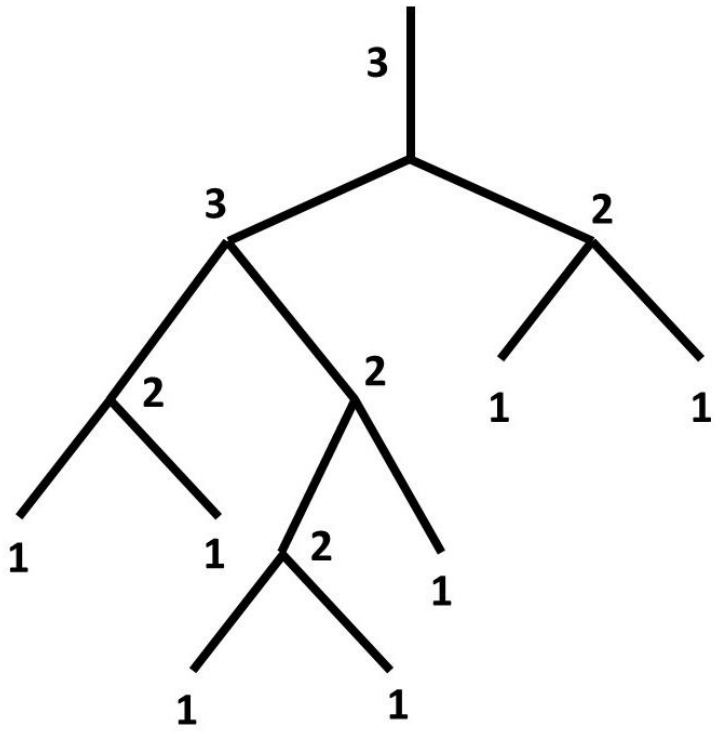

Figure 7-Schematic of the Strahler orders in a dichotomously branching system

From this study, the morphometric data show in TABLE 3 has been obtained.

TABLE 3-DATA ON THE PULMONARY ARTERIAL TREE [7]

Order	Number of branches	Diameter [mm]	Length [mm]	End branches
17	1.00	30.00	90.50	3.00e8
16	3.00	14.83	32.00	1.00e8
15	8.00	8.06	10.00	3.02e7
14	2.00e1	5.82	20.70	1.4e7
13	6.60e1	3.65	17.90	3.98e6
12	2.03e2	2.09	10.50	1.16e6
11	6.75e2	1.33	6.60	3.47e5
10	2.29e3	0.85	4.69	8.92e5
9	5.86e3	0.52	3.16	4.80e4
8	1.76e4	0.35	2.10	1.60e4
7	5.25e4	0.22	1.38	5.36e3
6	1.57e5	0.14	0.91	1.79e3
5	4.71e5	0.09	0.65	5.97e2
4	1.41e6	0.05	0.44	1.99e2
3	4.27e6	0.03	0.29	6.66e1
2	1.27e7	0.02	0.20	2.37e1
1	3.00e8	0.01	0.13	1.00

These data have been used in the current work as an anatomical reference for modelling the small arteries tree.

3.3 Computational procedure

As previously described, two main parts constitutes the current model: large arteries and small arteries. In the large arteries, values for blood flow and pressure are computed pointwise all along the branching network, while in the small arteries, the application of the simplified equations reported in Paragraph 3.2 allowed the computation of the input impedance, which in turn gives an appropriate outflow boundary condition for the large arteries. All the computation necessary for getting the solution of the problem were performed using MATLAB.

3.3.1 Input

The geometries for either large arteries or small arteries has been input in the analytical model for carrying out the solution. Large arteries data are reported in the form of a struct containing radii, lengths, and thickness; values for radii and lengths come from the processing of anatomical data as described in Paragraph 3.1.1. On the contrary, thickness have been approximated as a constant fraction of the radius (30%), to obtain not only reasonable values from an anatomical prospective, but also values compatible with the computational requirements in terms of meshing. The geometry of the large arteries was also characterized by the definition of the point in the space and the connectivity among them. Morphometric data reported in TABLE 3 gave all the needed information for building the structure of the small arterial tree. A matrix containing Strhaler order, diameter, length, thickness, area of the vessels' cross-section, was the other geometrical input of the analytical model. Thickness values were not found in literature, so another approximation has been used for obtaining values; the radius-to-thickness ratio $\left(\alpha = \frac{r}{h}\right)$ has been taken equal to 22, accordingly to what reported by Pollack et al. [28].

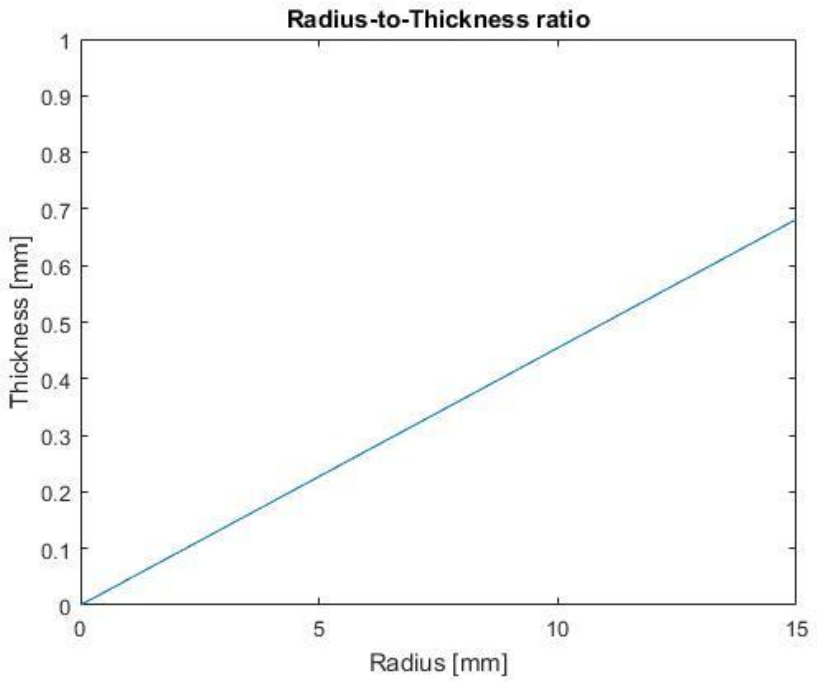

Figure 8-Radius-to-Thickness ratio plot according to Pollack et al.[28]

3.3.2 Parameter Definition

Material properties have been specified for the whole model; since the solution relies on the coupling of wall motion and fluid motion as described before, proper parameters both for arteries and blood have been used as an input to the model. Blood has been described as a Newtonian, incompressible fluid, characterized by the values reported in TABLE 4.

TABLE 4-BLOOD PROPERTIES

Variable	Symbol	Value
Density [kg/m^3]	ρ_b	1060
Viscosity [kg / (m · s)]	η_b	0.004

As far as the arteries are concerned, a viscoelastic model has been taken into consideration, which has been shown to have an important role in the wave propagation [38]. Viscoelasticity has the property of being frequency dependent, thus, the elastic modulus considered for the arteries is proportional to the frequency: the higher the frequency is, the higher the elastic modulus is. Such a characteristic can be described with a Voigt Model, shown in Figure 9, namely the parallel of a spring, related to the elastic component of the material, and a dashpot, which introduced the damping effect.

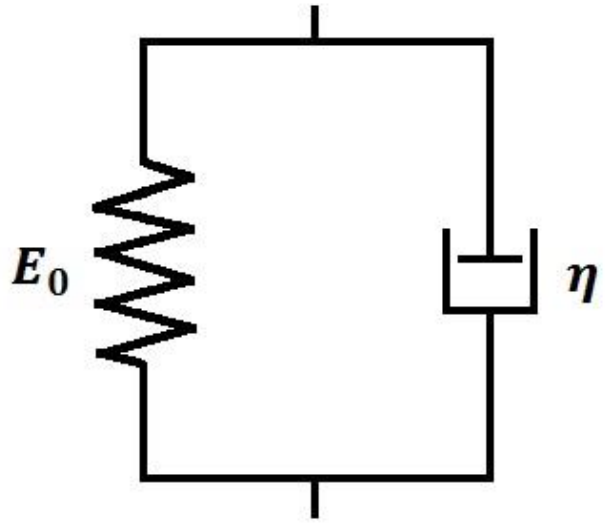

Figure 9-Voigt model (E_0 represents the spring, η represents the dashpot)

Using a Voigt model, one can write the elastic modulus in the following way:

Equation 41-Elastic Modulus according to Voigt Model

$$E = E_0 + i\omega\eta_w$$

Or in exponential form:

Equation 42-Elastic Modulus according to Voigt Model in exponential form

$$E = \sqrt{E_0^2 + (\omega\eta_w)^2}\exp\left(i\tan^{-1}\left(\frac{\omega\eta_w}{E}\right)\right)$$

Where:

- E_0 is the steady state elastic modulus, [Pa];
- η is the viscosity, [Pa · s];
- ω is the angular frequency, [rad/s].

The value of steady state elastic modulus and viscosity are assumed to be constant along the arterial tree and their values, taken from literature, are reported in TABLE 5.

TABLE 5-MATERIAL PROPERTIES OF THE ARTERIAL WALL

Variable	Symbol	Value
Steady State Elastic Modulus [Pa]	E	2.25e5 [28]
Viscosity [Pa · s]	η_w	3e3 [39]

The definition of the material properties of both blood and arterial wall provided all the information needed for the full characterization of the large arteries; for each segments values of resistance R, inertance L, capacitance C, characteristic impedance Z_0 and propagation coefficient γ were computed, accordingly to equations reported in Paragraph 3.1 and below.

$$R = \frac{\rho\omega}{\pi r^2 M}\sin\theta$$

$$L = \frac{\rho}{\pi r^2 M}\cos\theta$$

$$C = \frac{2(1-\upsilon^2)\pi {r_0}^2}{E}\frac{r_0}{h}$$

$$Z_0 = \sqrt{\frac{R + i\omega L}{i\omega C}}$$

$$\gamma = \sqrt{i\omega C(R + i\omega L)}$$

3.3.3 Outflow Boundary Condition Determination

While inflow boundary condition is known in term of pressure value, outflow boundary condition needs to be determined and its value equals the input impedance of the small arteries. For carrying out this computation, the order of the terminal segments of the large arteries is identified with a comparison with the morphometric data, and the branching network from that order to order 1 is approximated again with the morphometric data. Small artery segments of the same order are assumed to be identical and the branching pattern is considered to be dichotomous. With these simplifying assumptions, one can march back from order number one up to higher orders with the computation of the input impedance, knowing the terminal impedance. The starting point are the vessels of order 1, which terminal impedance is set to zero. Order-1 vessels input impedance results equal to:

Equation 43-Input impedance of vessels of order 1

$$Z(0, \omega) = \frac{i\, g^{-1} sin(\frac{\omega L}{c})}{cos\left(\frac{\omega L}{c}\right)}$$

This value of input impedance allows the computation of the terminal impedance of each parent vessel of order 2, claiming the parallel of two impedances and reminding the assumption of dichotomous branching.

Equation 44-Parallel of impedances

$$Z_{parent} = \frac{Z_{daughter1}\, Z_{daughter2}}{Z_{daughter1} + Z_{daughter2}}$$

Since segments of the same order are equal, one can write $Z_{daughter1} = Z_{daughter2}$, and find the value of the terminal impedance of the order 2, from the value of the input impedance of order 1 as follows:

Equation 45-Terminal impedance of order-2 vessel

$$Z_T(2) = \frac{Z_{in}^2(1)}{2Z_{in}(1)} = \frac{Z_{in}(1)}{2}$$

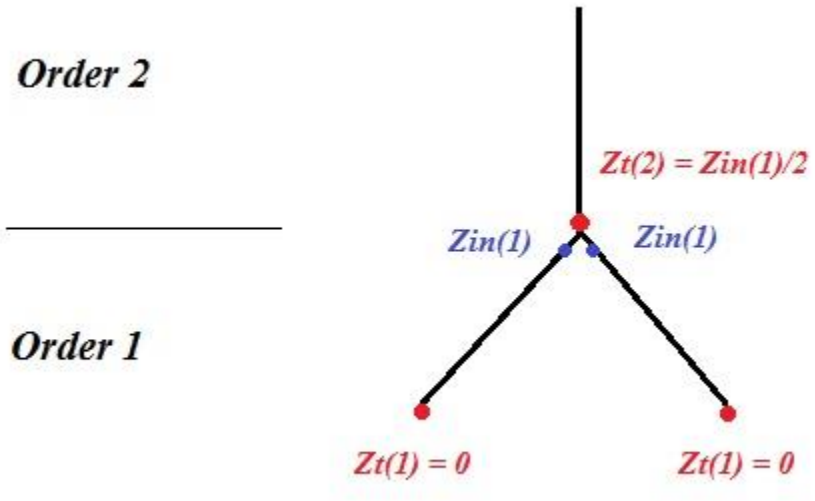

Figure 10-Terminal impedance of order-2 vessel

And more in general:

Equation 46- Terminal impedance of the parent vessel in small arteries

$$Z_T(n) = \frac{Z_{in}^2(n-1)}{2Z_{in}(n-1)} = \frac{Z_{in}(n-1)}{2}$$

The recursive application of Equation 40 and Equation 46 allows the computation of the input impedance all along the small artery tree. The input impedance of the small artery tree allows to obtain the terminal impedance of the large arteries, and in turn the outflow boundary condition is set up.

3.3.4 Large Arteries

The input impedance computation for the large arteries relies on the same procedure used for the small arteries: the only difference is in the equations used. Starting from the terminal impedance given by the input impedance of small arteries, the algorithm works upward, applying for each segment Equation 38 and Equation 44, reported below:

$$\begin{cases} Z_{in} = \dfrac{Z_T + Z_0 tanh(\gamma L)}{1 + \dfrac{Z_T}{Z_0} tanh(\gamma L)} \\ Z_{parent} = \dfrac{Z_{daughter1}\, Z_{daughter2}}{Z_{daughter1} + Z_{daughter2}} \end{cases}$$

Once reached the inlet of the pulmonary artery, the second boundary condition is applied, namely the know value of inlet pressure, which amplitude is set as the mean value of maximum systolic and diastolic pressure in Pascal.

TABLE 6-INLET BOUNDARY CONDITION IN TERMS OF PRESSURE

Variable	Value
P_{sys} [Pa]	4.00e3
P_{diast} [Pa]	2.00e3
P_{in} [Pa]	3.00e3

The application of the inlet boundary condition allows the algorithm to work downstream computing the pressure value all along the large artery three, through the use of Equation 39a:

$$P = P_{in}\left(\frac{Z_{in} + Z_0}{2Z_{in}} e^{-\gamma x} + \frac{Z_{in} - Z_0}{2Z_{in}} e^{\gamma x}\right)$$

At each bifurcation, the equation of continuity of pressure (Equation 10a) must be applied, in order to update the value of input pressure for each segment. The recursive application of this procedure allows the computation of the pressure in every point of the branching network.

CHAPTER 4

FINITE ELEMENT MODEL

To validate the built analytical model, a finite element model has been implemented in COMSOL® (COMSOL Multiphysics® v. 5.2a. www.comsol.com. COMSOL AB, Stockholm, Sweden). An acoustic-solid structure interaction has been carried out in the frequency domain, to obtain results to compare with the analytical model ones.

4.1 Mesh

The mesh used in COMSOL® for the acoustic simulation has been obtained from the same data for the large arteries used in the analytical model. These data have been processed in MATLAB in order to obtain a set of four files in .tcl (Tool Command Language) format, two for the inner point (end and non-end points) and two for the outer points (end and non-end points). These scripts have in turn been run in ANSYS ICEM CFD® (ANSYS® Academic Research, Release b17.2), generating two geometries, one for the outer points and one for the inner points. In each geometry, surfaces for inlet, outlet and wall have been meshed. The meshes parameters are reported in TABLE 7.

TABLE 7-MESH PARAMETERS

Max Global Element Seed Size	Min Size Curvature/Proximity Based Refinement
10	0.5

Once the two surface meshes have been obtained, they have been merged together. Two volumes have been added to the resulting mesh, one for the blood, and the other for the vessel thickness; volume elements were tetrahedra.

4.2 COMSOL® Simulation

An acoustic-solid structure interaction simulation in the frequency domain has been performed in COMSOL®. The mesh created in ICEM CFD® was imported and generated the geometry for the finite element study. Boundaries were defined at the inlet, at the outlet and in correspondence of the annulus of the main pulmonary artery. Blood and thickness were defined as two domains: blood has been analyzed in terms of acoustics, while thickness in terms of solid mechanics. The properties for blood and thickness, specified in the model are reported in TABLE 8 and in TABLE 9.

TABLE 8-BLOOD PROPERTIES FOR THE FE MODEL

Property	Symbol	Value
Density [kg/m^3]	ρ_b	1060
Speed of sound [m/s]	c_b	1570

TABLE 9-ARTERIAL WALL PROPERTIES FOR THE FE MODEL

Property	Symbol	Value
Young's Modulus [Pa]	E	$2.25e5 + i\omega 3e3$
Poisson's Ratio [-]	υ	0.45
Density [kg/m^3]	ρ_w	1160

In the acoustics module, relative to blood, the amplitude of the pressure at the inlet boundary was set to be 3.00e3 Pa. A value of impedance was specified too, in order to obtain a second boundary condition: the terminal impedances of the terminal segments were set to be equal to the values obtained from the analytical model, which are reported in TABLE 10 for each frequency, times the area of the vessels' cross-section, computed as $A_{mean} = \pi r_{mean}^2 = 1.74 * 10^{-4}\ m^2$.

TABLE 10-TERMINAL IMPEDANCES FOR EACH FREQUENCY USED AS BOUNDARY CONDITION IN FE MODEL

Frequency [Hz]	**Terminal Impedance [Pa·s/m^3]**		**Specific Terminal Impedance [Pa·s/m]**	
	Real	**Imag**	**Real**	**Imag**
1	1.70e7	-1.78e8	2.96e3	-3.10e4
5	1.71e7	-2.80e7	2.98e3	-4.88e3
10	1.97e7	-2.55e6	3.43e3	-4.44e2
15	2.41e7	9.19e6	4.20e3	1.60e3
50	4.27e7	3.35e7	7.44e3	5.83e3
100	5.76e7	5.12e7	1.00e4	8.93e3

In the solid mechanics module, a condition on the annulus boundary has been specified: the main pulmonary artery annulus was considered to be a fixed constrain, namely its displacement was set to be equal to zero.

CHAPTER 5

RESULTS

Different simulations have been performed using the approaches explained before. In a first place, a simple case has been analyzed. In this part, just seven arteries have been taken into consideration, and the input pressure has been considered a sinusoid. Secondly, at the inlet of the main pulmonary artery, the boundary condition was defined as a pressure of the form of pulse wave. Finally, sickle cell disease and pulmonary hypertension have been simulated.

5.1 Preliminary study

A first simulation of wave propagation has been performed in a simplified pulmonary arterial tree, which considered only three bifurcations, thus seven segments: main pulmonary artery, right and left pulmonary artery, and the four lobar arteries (two upper and two lower).

5.1.1 Analytical Model

The one-dimensional geometry of the analytical model is reported in Figure 11:

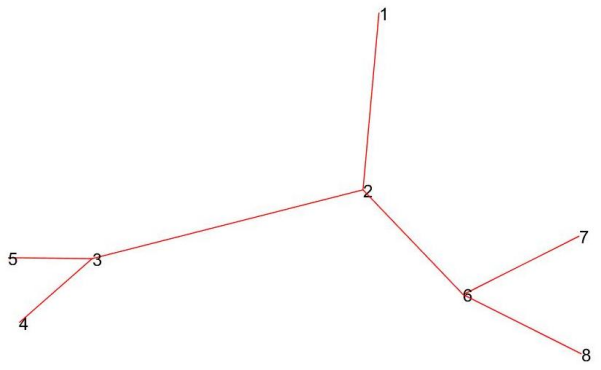

Figure 11-Simple Tree for the analytical model

In Figure 11, each point constituting the tree is labeled with a number and the connection between them is specified in a connectivity matrix, which associates to each couple of points a segment. The connectivity matrix is shown in TABLE 11.

TABLE 11-CONNECTIVITY MATRIX

Segment Number	**Starting point**	**Ending point**
1	1	2
2	2	3
3	3	4
4	3	5
5	2	6
6	6	7
7	6	8

As said before, this connectivity matrix encodes the connection between the points and between the segments, in order to be able to reconstruct the branching network. For example, segment 1 goes from point 1 to point 2, and it is connected to segment 2, which goes from point 2 to point 3, and segment 5, which goes from point 2 to point 6: proceeding with this approach all the way down the tree, its structure can be reconstructed.

Radius, length, and thickness values are specified for each segment of the tree, and in this simulation their values are the one reported in TABLE 12.

TABLE 12-RADIUS, LENGTH, THICKNESS OF EACH SEGMENT CONSTITUTING THE TREE

Segment Number	Radius [mm]	Length [mm]	Thickness [mm]
1	11.98	97.38	3.99
2	10.57	130.73	3.52
3	6.92	42.73	2.31
4	8.83	38.72	2.94
5	9.54	74.40	3.18
6	5.43	59.76	1.81
7	8.60	65.28	2.87

With this procedure, the tree is fully characterized from a geometrical point of view, and along with the definition of the material properties, specified in Paragraph 3.3.2, all pieces of information for the analytical model are provided. The values of pressure have been computed over 1000 points along each vessel, and the results have been evaluated in terms of real part of the pressure and magnitude of the pressure in logarithmic scale. Six frequencies have been considered in the first place: 1 Hz, 5 Hz, 10 Hz, 50 Hz, 100Hz. The inlet pressure amplitude was set to a value of 3.00e3 Pa: this means that each simulation had as inflow boundary condition a sinusoid with this amplitude and a frequency of 1Hz, 5Hz, 10Hz, 15Hz, 50Hz, 100Hz respectively. The results are visualized in Figure 12 and Figure 13, both for the real part in [Pa], and for the magnitude in [dB].

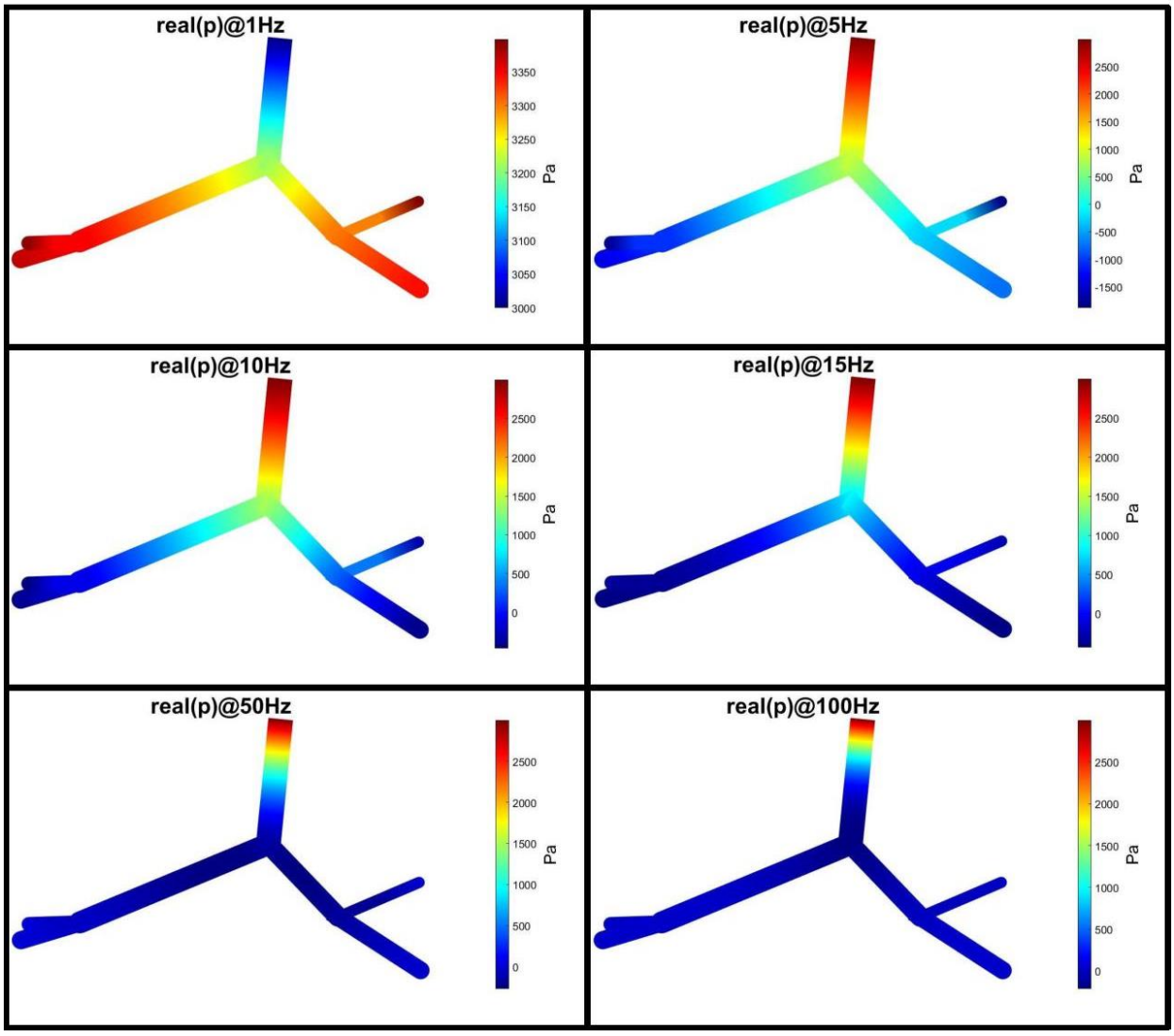

Figure 12-Real part of the pressure [Pa] from the analytical model (frequency 1Hz, 5Hz, 10Hz, 15Hz, 50Hz, 100Hz)

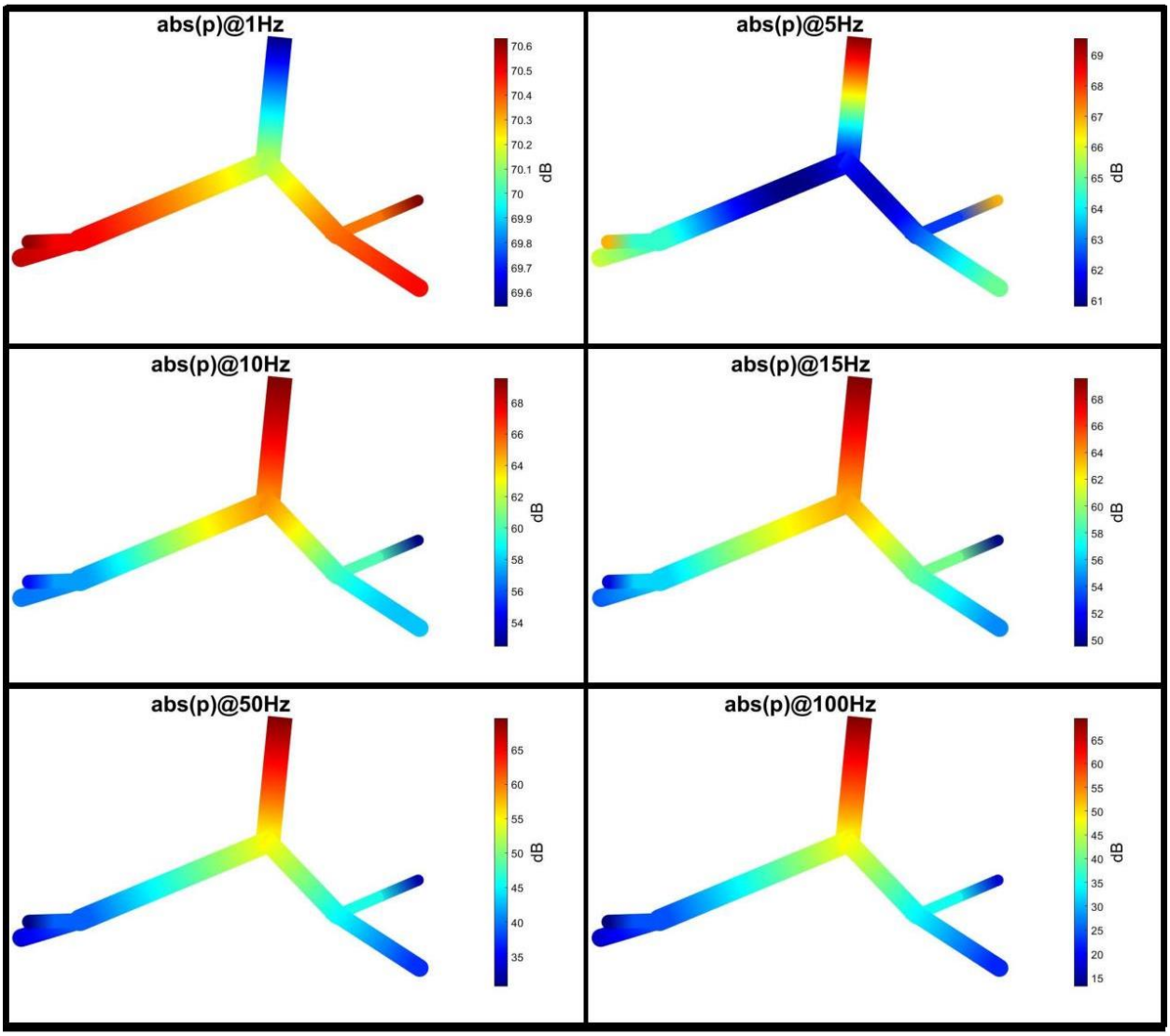

Figure 13-Magnitude of the pressure [dB] from the analytical model (frequency 1Hz, 5Hz, 10Hz, 15Hz, 50Hz, 100Hz)

5.1.2 Finite Element Model

The analytical model geometry was the starting point for building the mesh necessary for the finite element analysis: the procedure to obtain the mesh is reported in Paragraph 4.1. In Figure 14 reported the meshes for blood domain and thickness domain made in ICEM CFD®.

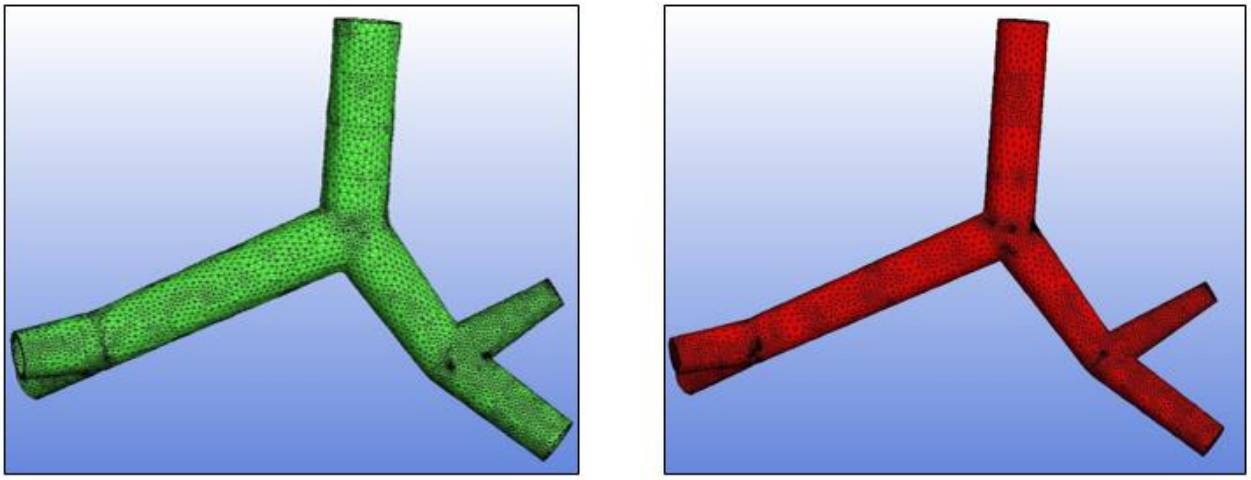

Figure 14 - ICEM CFD® mesh (green = thickness domain, red = blood domain)

The mesh built in ICEM CFD®, was then imported in COMSOL®, where the finite element analysis was performed.

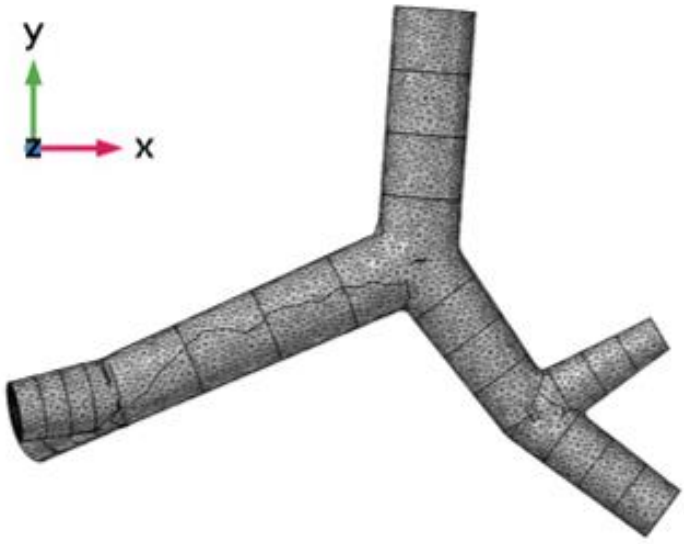

Figure 15-COMSOL® mesh

The finite element simulation in COMSOL® has been performed as explained in Paragraph 4.2, for the same frequencies used in the analytical model, namely 1Hz, 5Hz, 10Hz, 15Hz, 50Hz,

100Hz. The obtained results were still represented in terms of real part of the pressure in [Pa] and in terms of magnitude in logarithmic scale [dB], and are reported in Figure 16 and Figure 17.

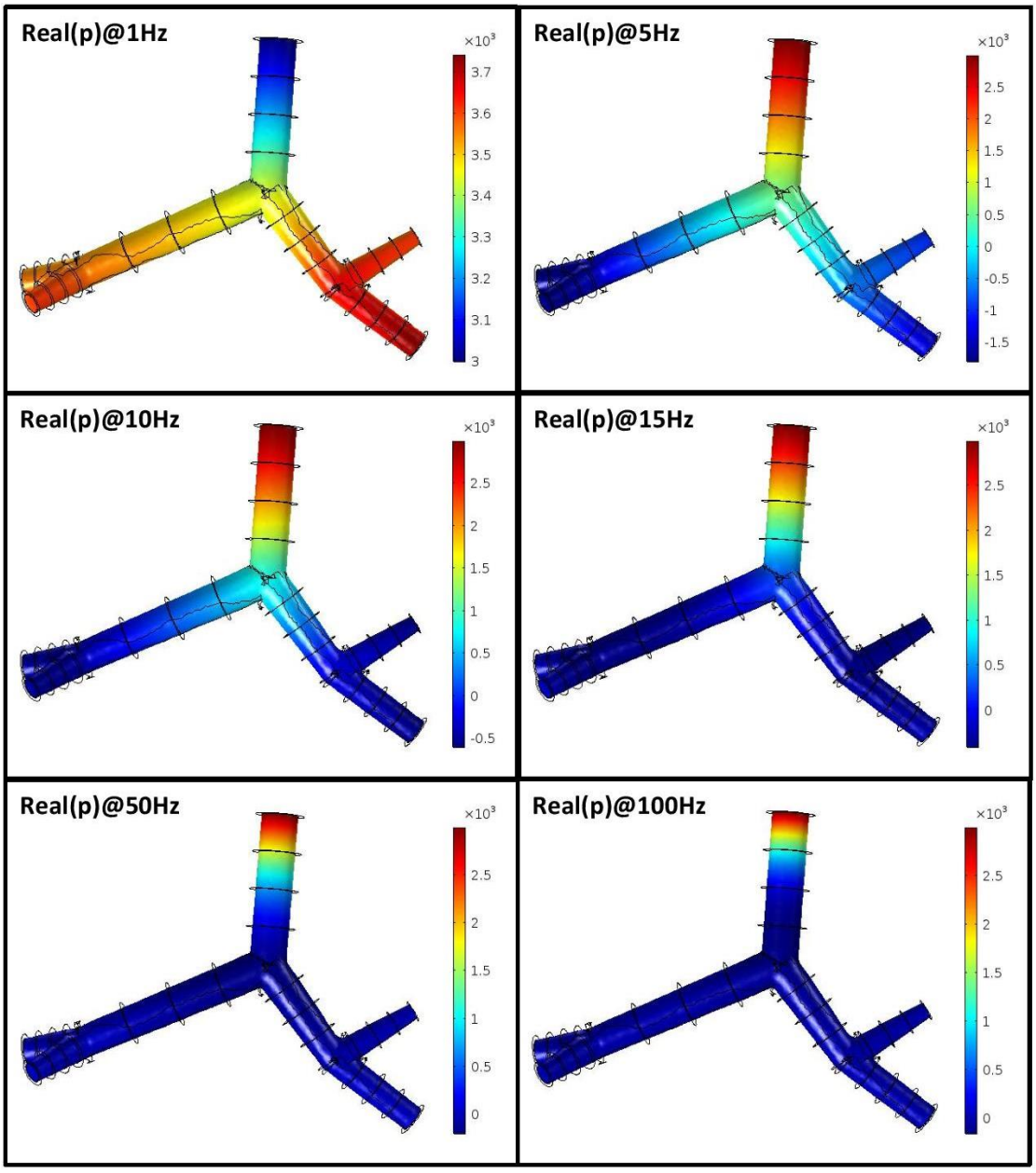

Figure 16-Real part of the pressure [Pa] from the FE model (frequency 1Hz, 5Hz, 10Hz, 15Hz, 50Hz, 100Hz)

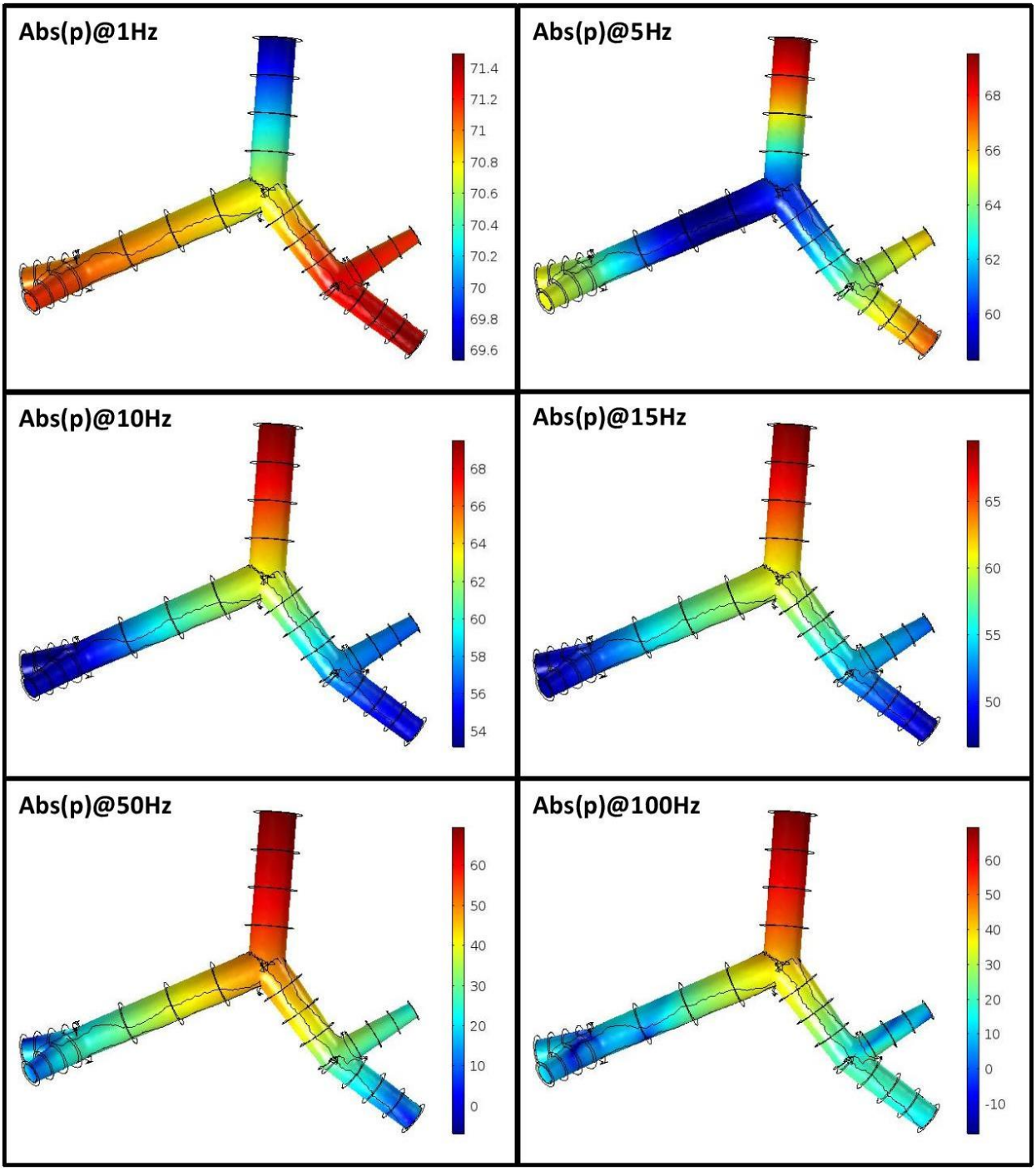

Figure 17-Magnitude of the pressure [dB] from the FE model (frequency 1Hz, 5Hz, 10Hz, 15Hz, 50Hz, 100Hz)

5.1.3 Error Analysis

The validation of the analytical model relies on the comparison with the finite element model. In the first place, the pressure plot (real part of the pressure and magnitude in dB) of both models were compared for having a qualitative representation of how the two models performed with respect to each other. The comparison between the two models is shown in Figure 18, Figure 19, Figure 20, and Figure 21.

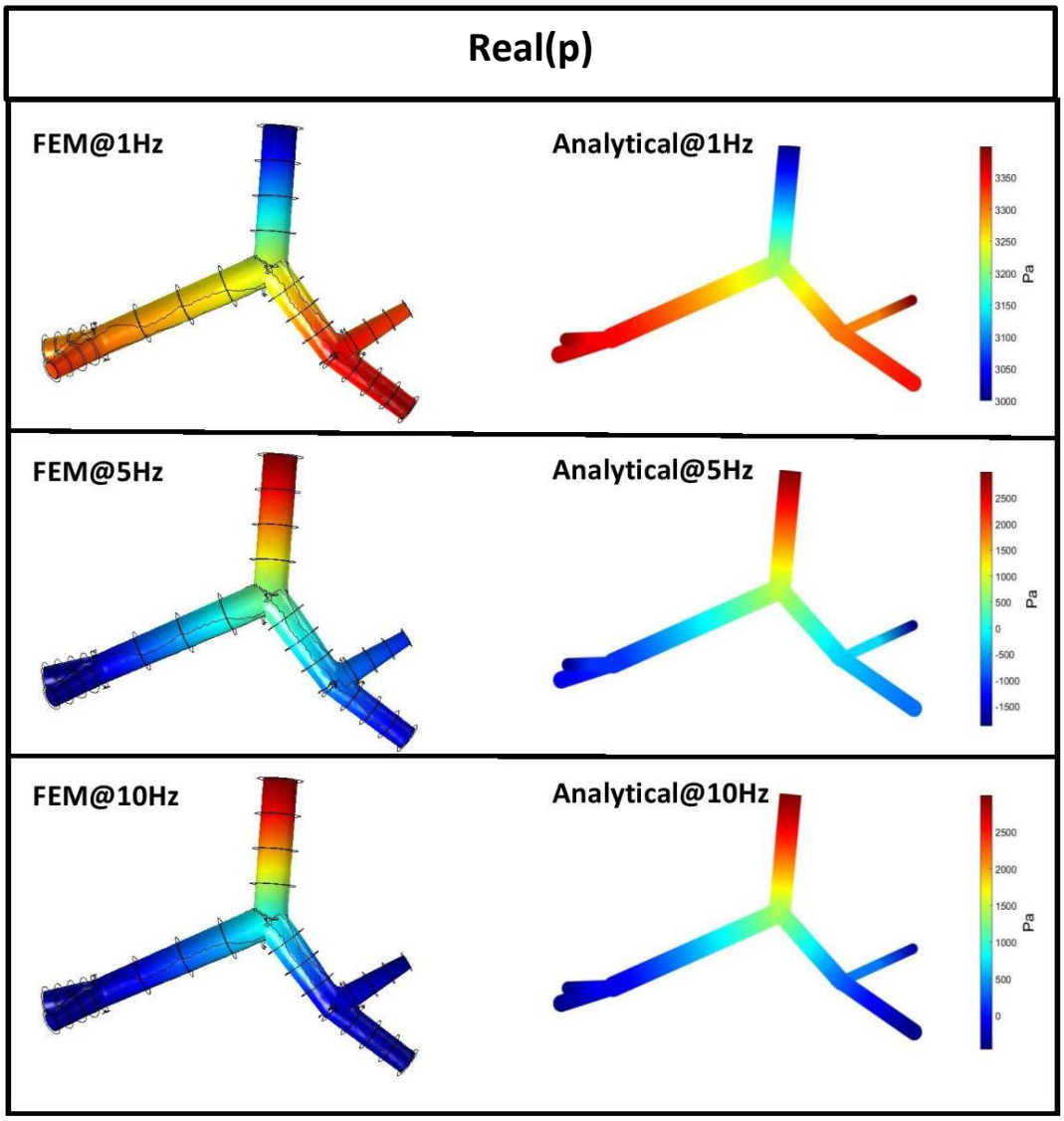

Figure 18-Comparison of FE and analytical model real part of the pressure at f = 1Hz, 5Hz, 10Hz

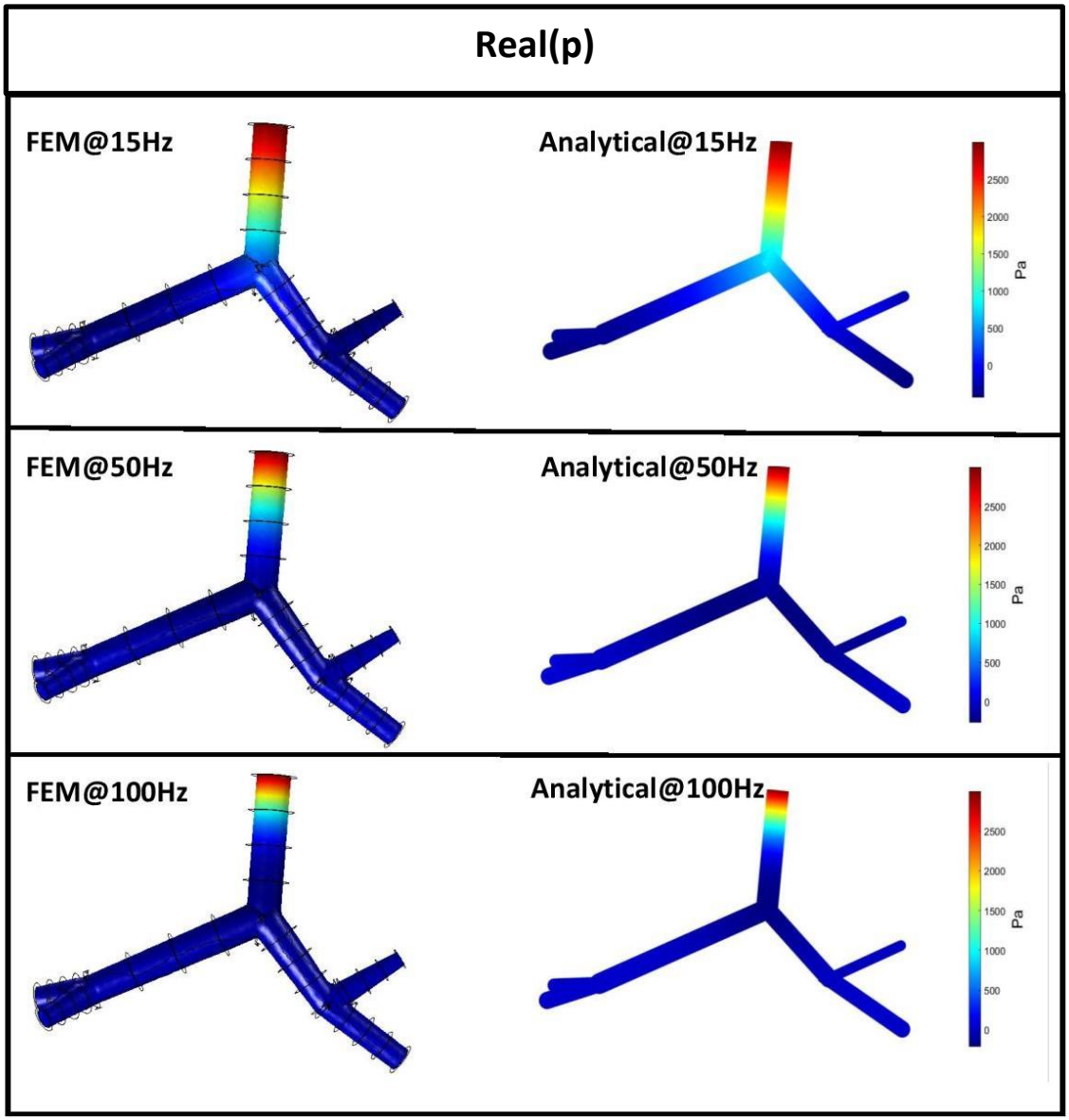

Figure 19-Comparison of FE and analytical model real part of the pressure at f = 15Hz, 50Hz, 100Hz

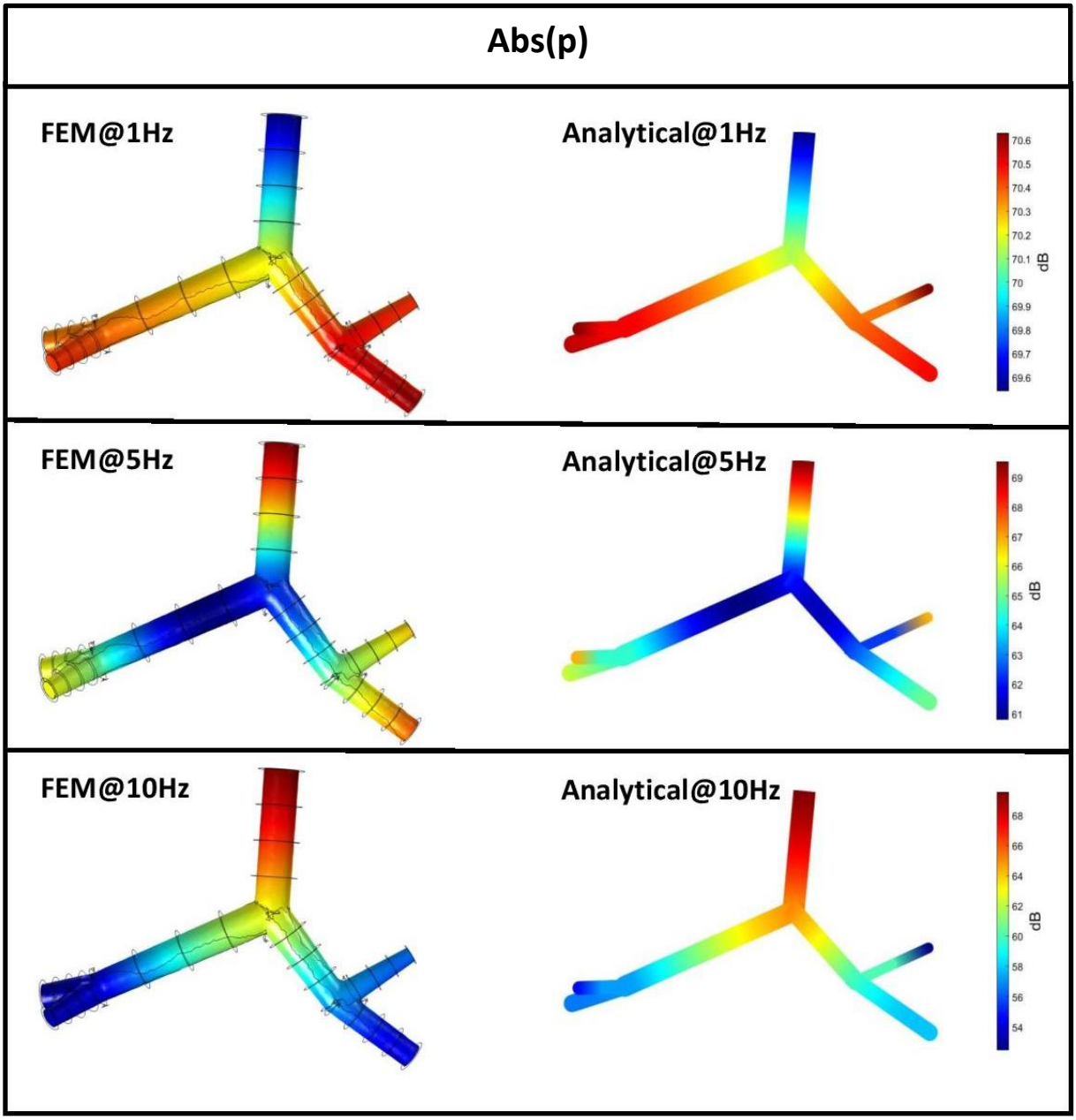

Figure 20-Comparison of FE and analytical model magnitude of the pressure at f = 1Hz, 5Hz, 10Hz

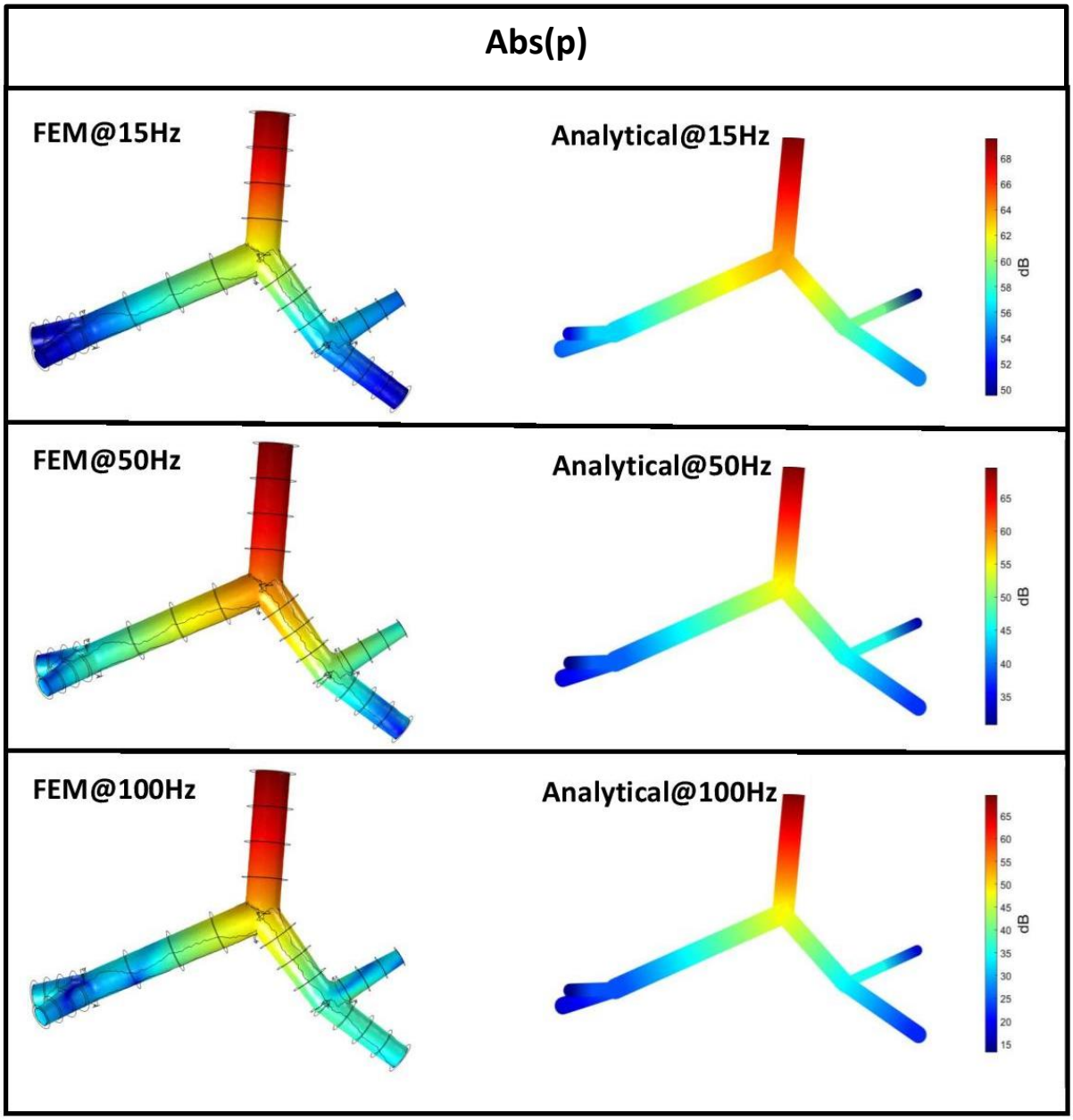

Figure 21-Comparison of FE and analytical model magnitude of the pressure at f = 15Hz, 50Hz, 100Hz

For a more quantitative evaluation of the relative performances of the models, the magnitude in logarithmic scale has been numerically compared, with the computation of the relative percent error as follows:

Equation 47-Relative error percent

$$error = \left|\frac{Analytical - FEM}{Analytical}\right| * 100$$

Where:

- $Analytical = 20\log_{10}|P_{analytical}|$, [dB];
- $FEM = 20\log_{10}|P_{FEM}|$, [dB].

This computation has been performed in MATLAB, and in order to do that, the results from COMSOL® needed to be exported. For having the best accuracy, the values have been evaluated in the same points in both models, namely each segment of the FE model was divided in 1000 points placed in the same position of the points in the analytical model, as it is shown in Figure 22.

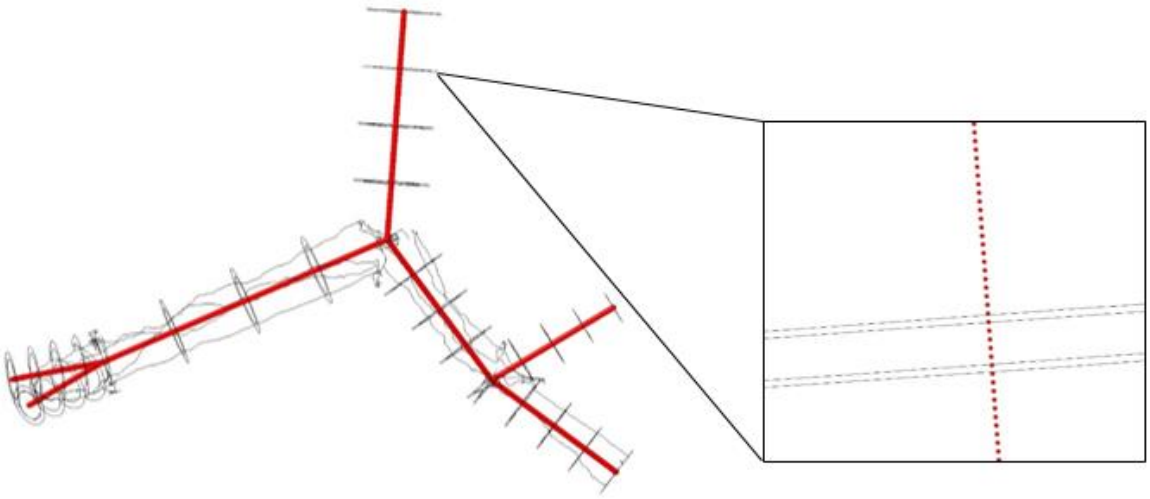

Figure 22 - Point distribution in COMSOL®

Once the results were exported form COMSOL® and imported in MATLAB, the error analysis has been performed and the results are shown in the plots reported in Figure 23.

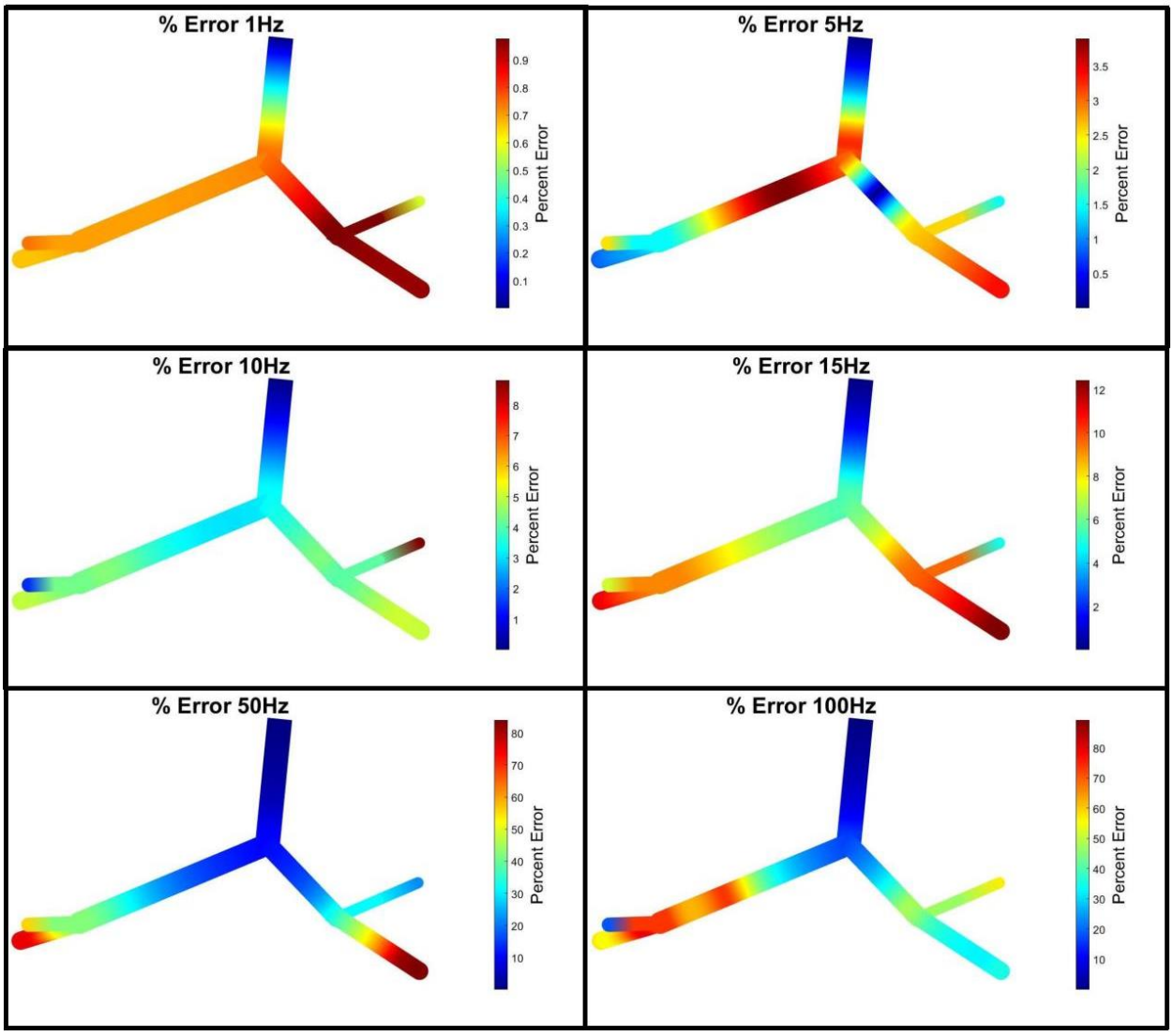

Figure 23 - Plot of percent error for f = 1Hz, 5Hz, 10Hz, 15Hz, 50Hz, 100Hz

A histogram was plotted too at each frequency to visualize the error distribution, as shown in the graph from Figure 24 to Figure 29.

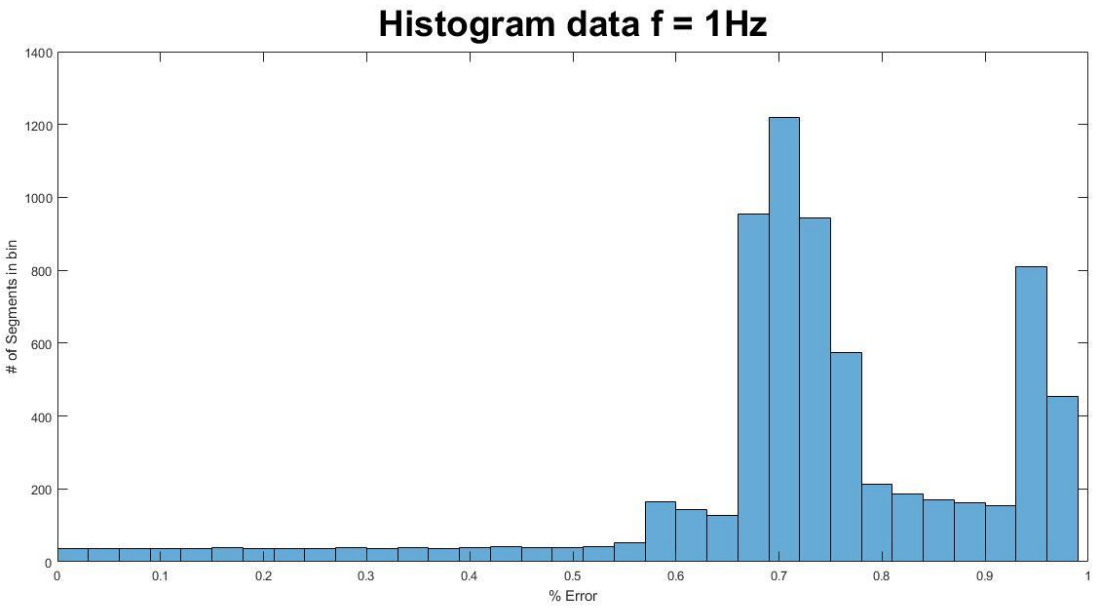

Figure 24 - Histogram of the percent error at f = 1Hz

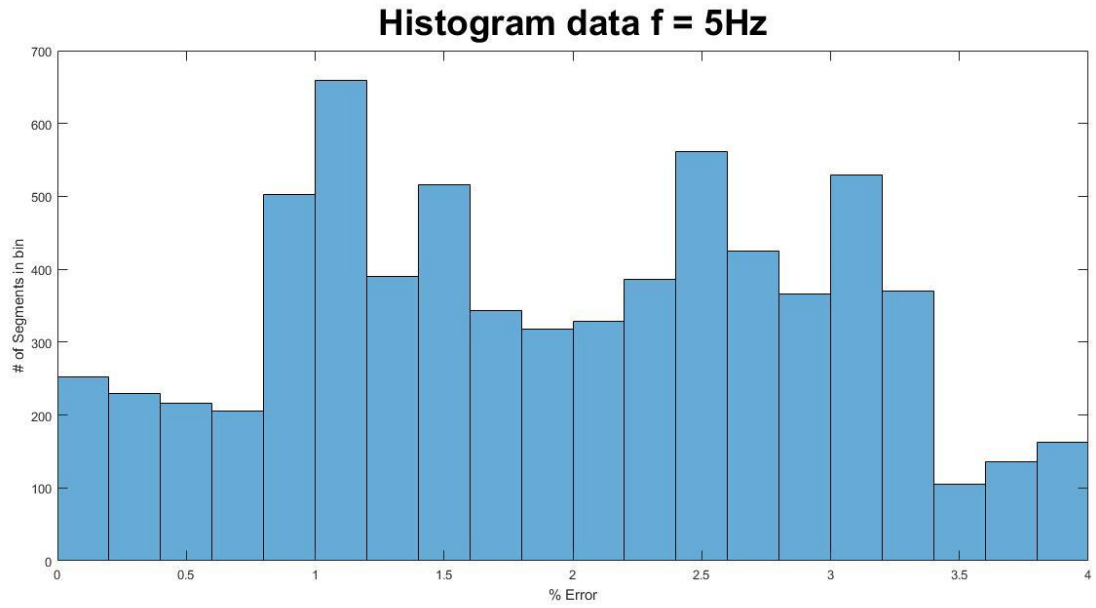

Figure 25 - Histogram of the percent error at f = 5Hz

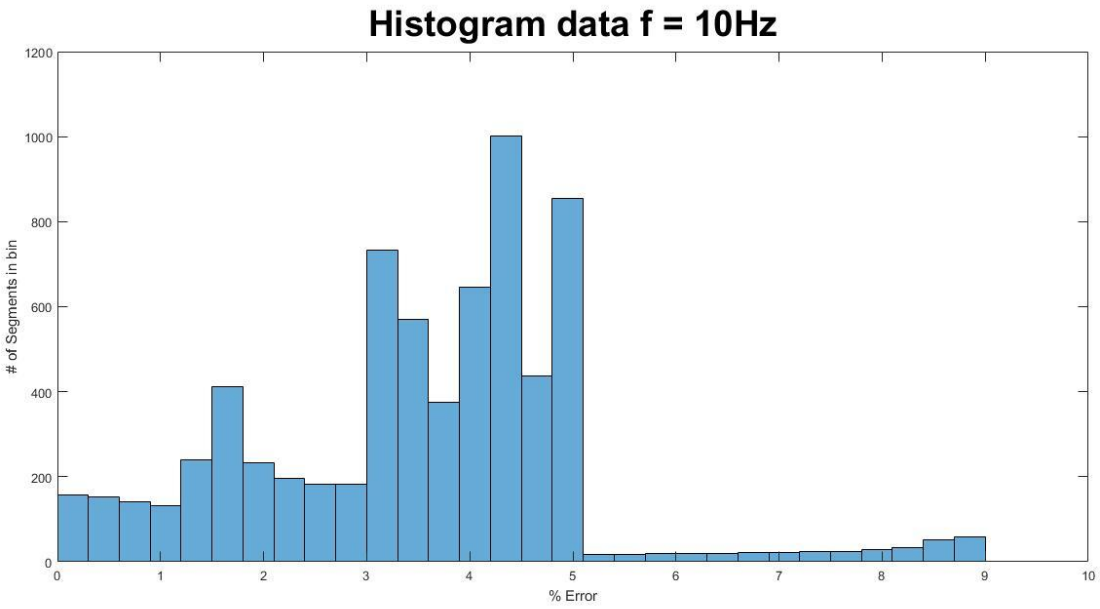

Figure 26 - Histogram of the percent error at f = 10Hz

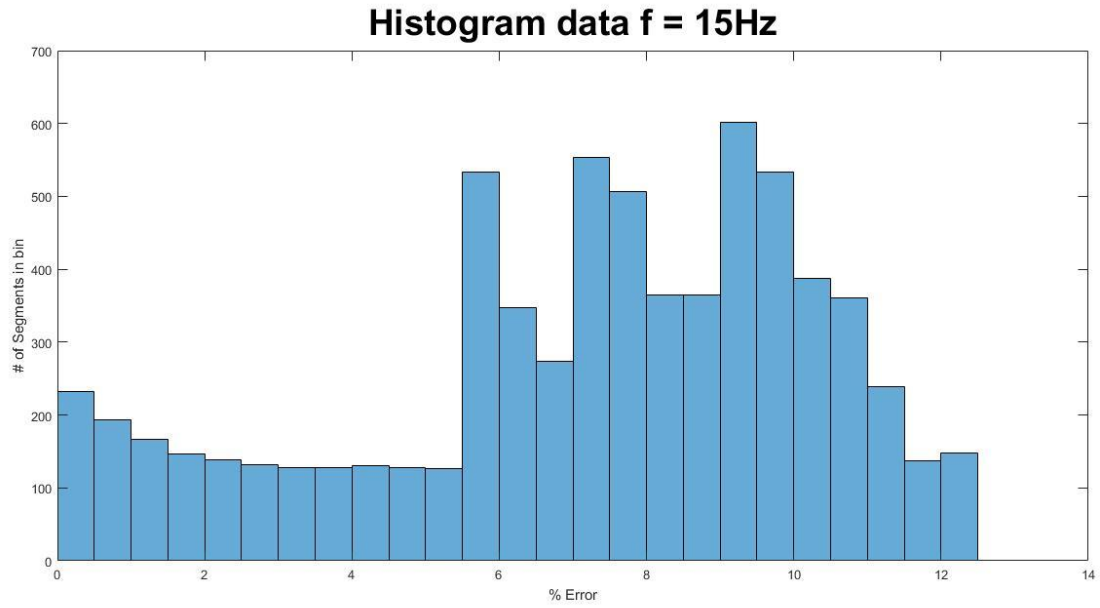

Figure 27 - Histogram of the percent error at f = 15Hz

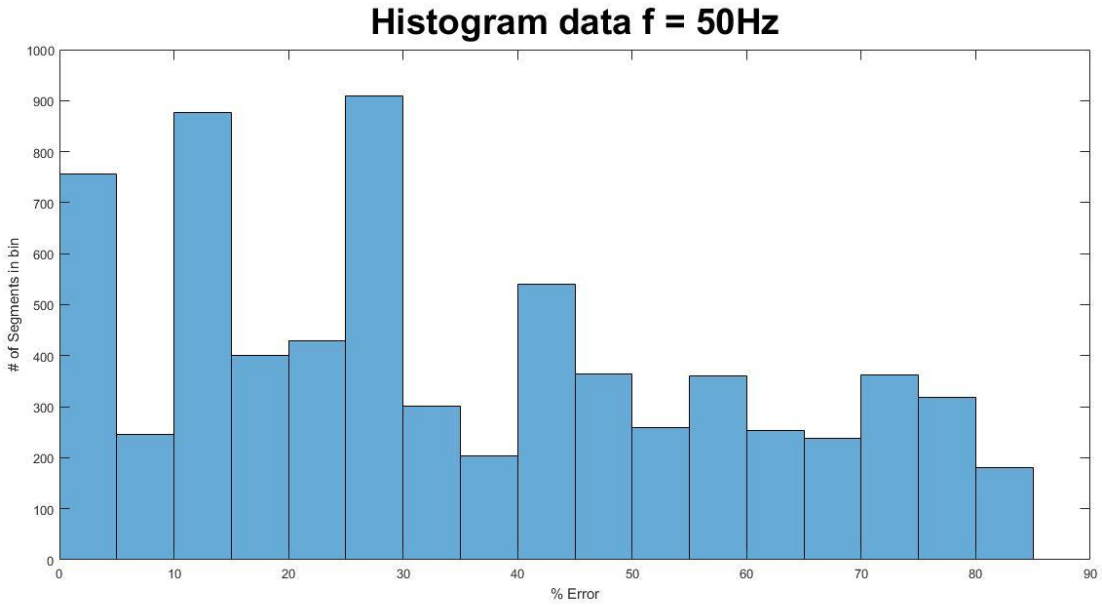

Figure 28 - Histogram of the percent error at f = 50Hz

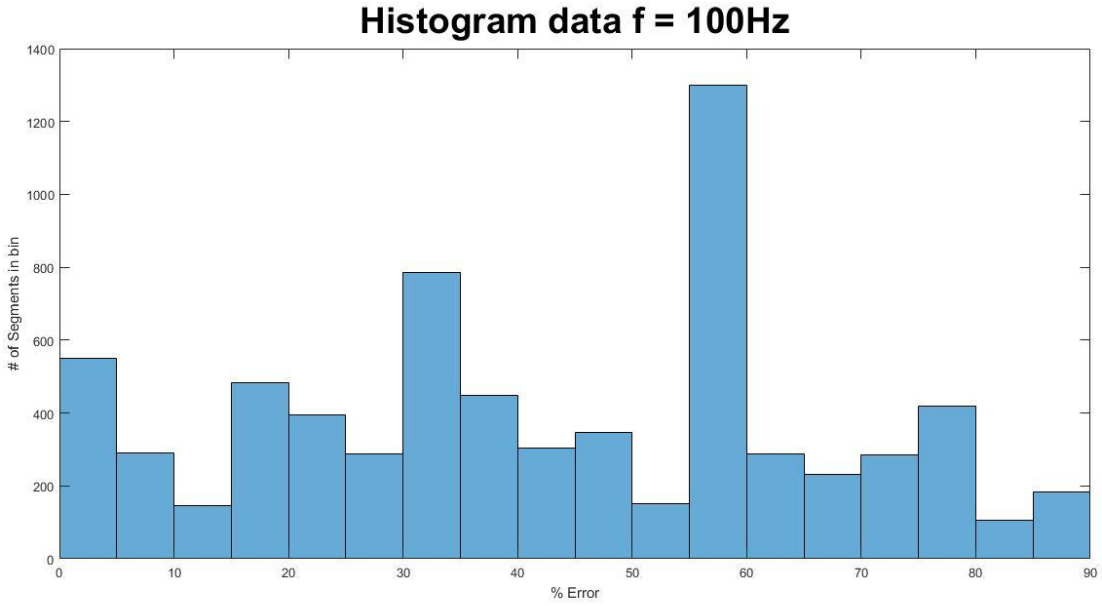

Figure 29 - Histogram of the percent error at f = 100Hz

The mean error for each frequency are reported in TABLE 13.

TABLE 13 - MEAN PERCENT ERROR FOR EACH FREQUENCY ANALYZED

Frequency [Hz]	**Mean Percent Error [%]**
1	0.72
5	1.93
10	3.5
15	7.12
50	35.00
100	42.47

From the comparison between analytical and finite element model, quite a good agreement can be noticed. From a qualitative point of view, the plots of the real part of the pressure look similar, which means that in both model the propagation of the pressure behaves in the same way. Quantitatively, the error analysis shows that the values of pressure magnitude in [dB] are reasonably comparable between the two models: the maximum mean error is 42.47% at 100Hz. From the results, one can notice that the higher the frequency, the higher the error. Also, the distributions of the error along the arterial tree show a higher error in the terminal branches; this can be associated with the recursive nature of the algorithm, that from a known value of pressure at the inlet of the main pulmonary artery computes all the pressure values downstream. It is reasonable then that near the inlet the error is minimum, being closer to the imposed boundary condition, while away from the inlet the error increases due to the summation of recursive computation. The qualitative and the quantitative comparison show a good agreement between the two models and this validates the analytical model.

5.2 Pulse wave simulation

The validation of the analytical model confirms its reliability and further simulation can be carried out with this tool. The analytical model allows to obtain solution in the frequency domain with sinusoidal input. The pressure pulse wave generated by the right ventricle has been simulated by superposition principle: each harmonic composing the pulse wave has been used as an inlet boundary condition for the analytical model and solutions for each harmonic have been summed. The frequency content of the pulse wave has been taken from literature [1], where information about only the first two harmonics were found. Figure 30 shows the spectrum of the pulse wave.

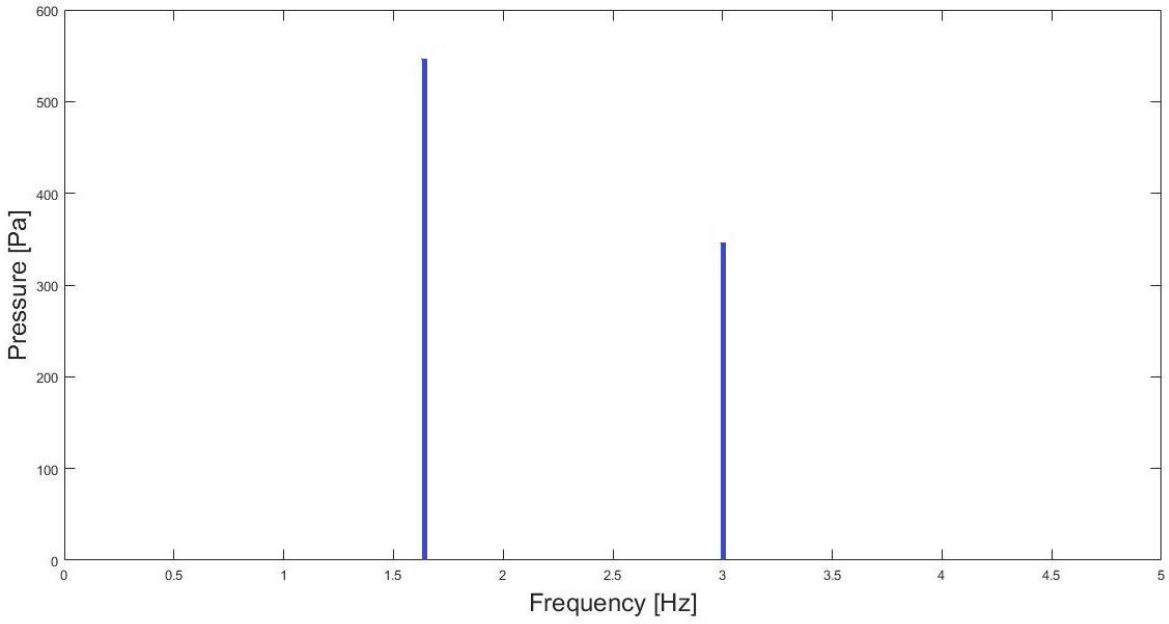

Figure 30-Frequency content of the pressure pulse wave

The values of frequency and amplitude of the pressure spectrum are reported in TABLE 14.

TABLE 14 - FREQUENCY SPECTRUM OF THE PRESSURE PULSE

Harmonic	Frequency [Hz]	Amplitude [Pa]	Phase Shift [rad]
1	1.5	550	0.49
2	3	350	1.11

Starting from this spectrum, the analytical model has been run two times, each time having a single harmonic as input pressure at the inlet of the main pulmonary artery. The phase shift has been taken into consideration using a complex-valued pressure as input, of the from reported in the equation below:

Equation 48 - Complex-valued input pressure

$$P_{in-i} = A_i e^{i\theta_i}$$

where:

- P_{in-i} is the input pressure for the i-th harmonic;
- A_i is the amplitude of the i-th harmonic;
- θ_i is the phase shift of the i-th harmonic.

Once the solution has been obtained for each harmonic, the pressure in the time domain has been computed as follows.

Equation 49 - Summation of the weighted pressure for each harmonic

$$p(t) = \sum_{i=1}^{N} P_i \sin(\omega_i t)$$

With:

- P_i is the pressure computed for the i-th harmonic.

- N = number of harmonics;
- $\omega_i = 2\pi f_i$, where f_i is the frequency of the i-th harmonic.

The time interval was taken from zero to the double of the period of the fundamental frequency, namely 1.64Hz.

Equation 50-Fundamental period of the pulse wave

$$T = \frac{1}{f} = \frac{1}{1.64Hz} = 0.61\ s$$

The time interval was then built as a vector from zero to 1.22 sec, discretized in 1000 points. A point in the middle of the main pulmonary artery has then been considered, and the pressure at that point has been plotted in the time interval considered; the result is shown in Figure 31.

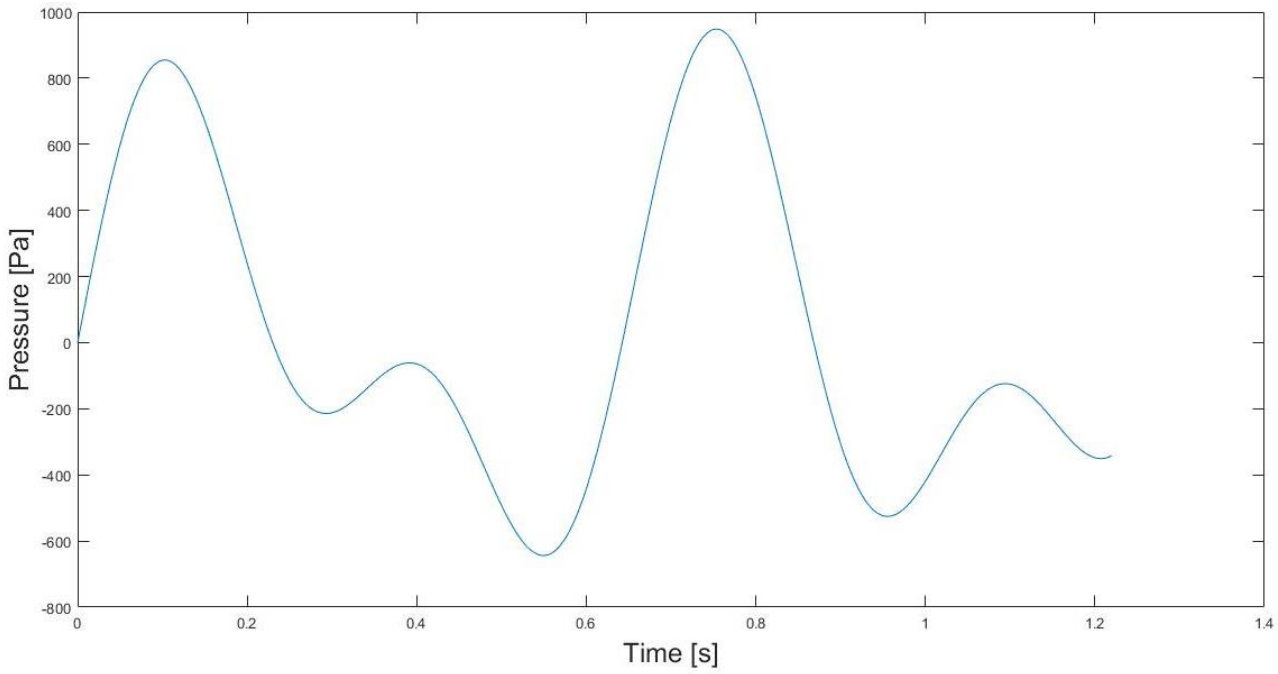

Figure 31 – Sum of the first two harmonics in the time domain plotted over two periods

5.3 Pathology simulation

Sickle cell disease and pulmonary hypertension have also been simulated with the analytical model. As explained in the introduction chapter, one of the complication of sickle cell disease is vaso-occlusion: rigid sickle-shaped erythrocytes get stuck in the microcirculation, causing ischemia. Vaso-occlusion has been simulated with an increase in the terminal impedance at the level of the arterioles. The terminal impedance has been increased of a factor 10^5. Vaso-occlusion, together with hemolytic anemia, can trigger the development of pulmonary hypertension, which leads to vascular remodeling, that increase stiffness and thickness of the arterial wall. Stiffening and thickening of the arterial wall can be simulated with the analytical model increasing the corresponding parameters, namely thickness and Young's modulus. For this purpose, thickness of the arterial wall has been multiplied times a factor 1.5: increasing thickness of the wall means narrowing of the vessel lumen, so un the pathology simulation the radius has been decreased of an amount equal to the new computed thickness.

Equation 51-Values of thickness and radius for pathology simulation

$$\begin{cases} Thickness_{Pathology} = 1.5 * Thickness_{Healthy} \\ Radius_{Pathology} = Radius_{Healty} - Thickness_{Pathology} \end{cases}$$

As far as the stiffness is concerned, the Young's modulus has been increased by a factor 10.

Equation 52-Young's modulus for the pathology simulation in [Pa]

$$E_{Pathology} = 10 * E_{Healthy} = 2.25e6 + i\omega 3e4$$

The solutions have been computed in terms of real part of the pressure for 5 frequencies, both for the healthy and the pathologic one: 1Hz, 10Hz, 100Hz, 500Hz. The results obtained are reported in Figure 32 and Figure 33.

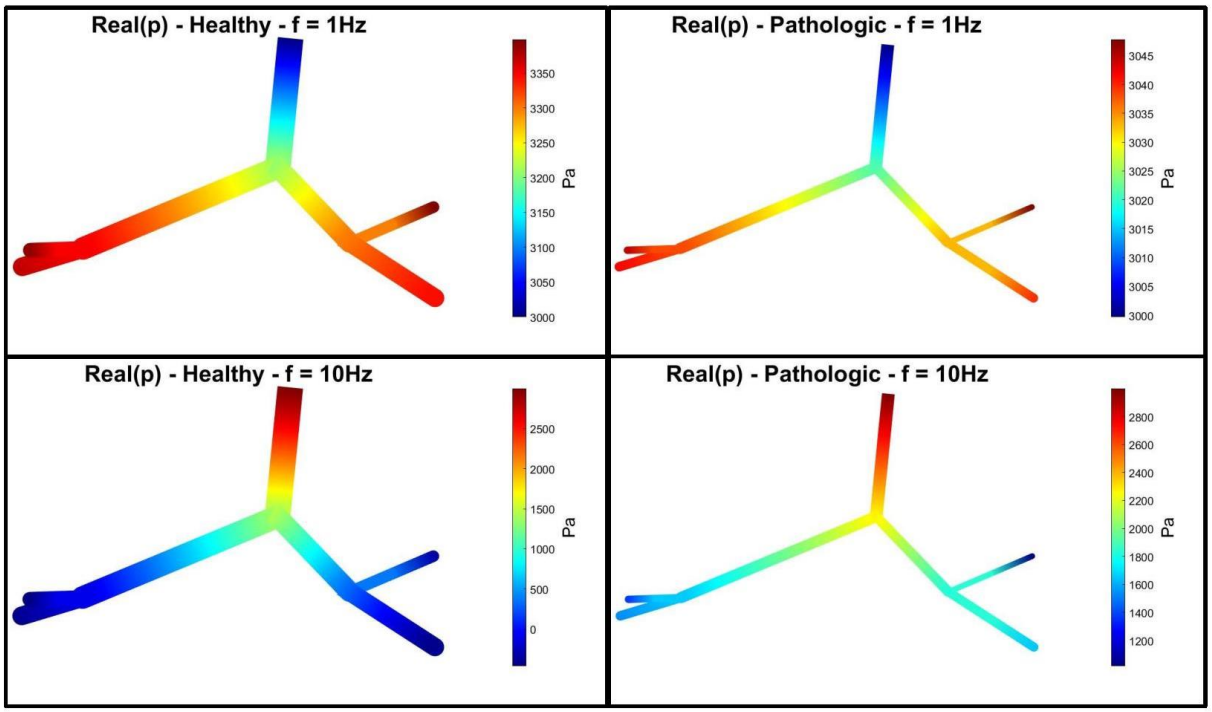

Figure 32 - Real part of pressure in healthy and pathologic case at f = 1Hz, 10Hz

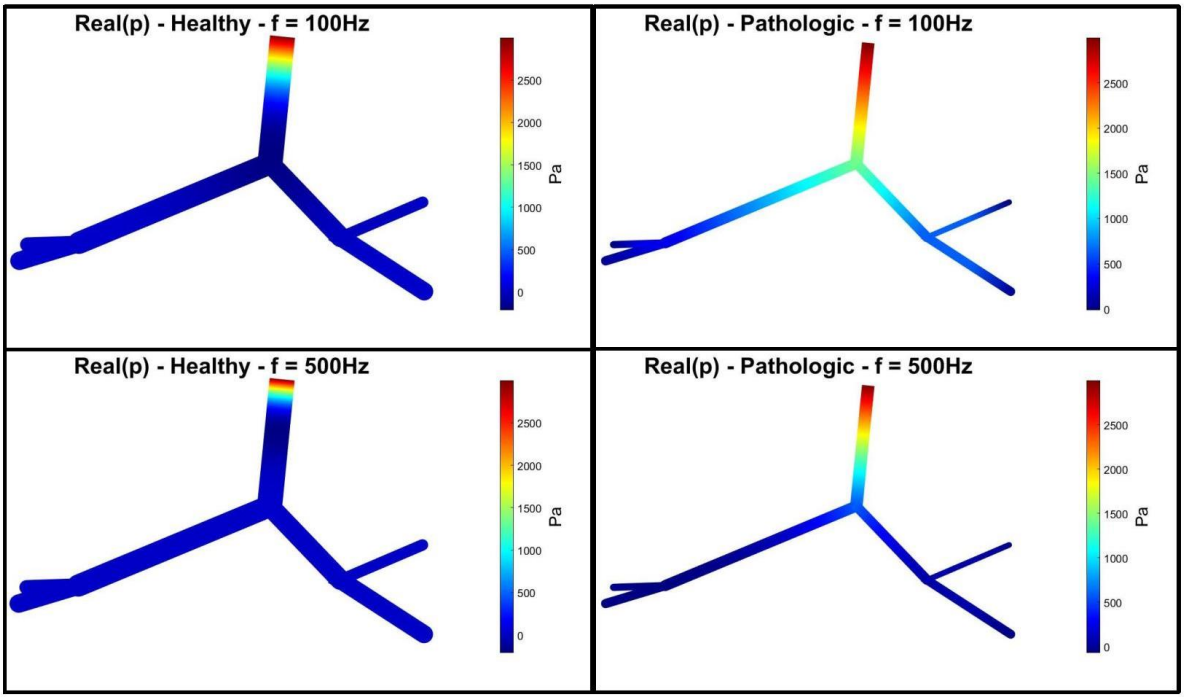

Figure 33 - Real part of pressure in healthy and pathologic case at f = 100Hz, 500Hz

The healthy and pathological case have also been studied in terms of phase velocity. Reminding Equation 6, the phase velocity is defined as:

Equation 53-Phase velocity

$$v_p = \frac{\omega}{\beta} = \lambda f$$

TABLE 15-VALUES OF PHASE VELOCITY FOR EACH SEGMENT AT EACH FREQUENCY CONSIDERED (H = HEALTHY, P = PATHOLOGIC)

	Phase Velocity [m/s]							
Segment	**1Hz**		**10Hz**		**100Hz**		**500Hz**	
	H	**P**	**H**	**P**	**H**	**P**	**H**	**P**
1	6.40	33.70	8.02	43.56	25.86	141.57	60.25	330.01
2	6.36	33.36	8.01	43.46	25.85	141.55	60.25	330.01
3	6.21	32.09	7.97	43.05	25.85	141.50	60.25	330.01
4	6.31	32.84	8.00	43.31	25.85	141.53	60.25	330.01
5	6.33	33.07	8.00	43.38	25.85	141.54	60.25	330.01
6	6.10	31.27	7.94	42.75	25.84	141.48	60.25	330.02
7	6.30	32.76	7.99	43.28	25.85	141.53	60.25	330.01

For having a better idea of the phase velocity trend, the mean phase velocity for each frequency both for healthy and for pathologic case has been computed, and it is reported in TABLE 16.

TABLE 16-MEAN PHASE VELOCITY FOR HEALTHY AND PATHOLOGIC CASE

Frequency [Hz]	Mean Phase Velocity [m/s]	
	Healthy	Pathologic
1	6.29	32.73
10	7.99	43.26
100	25.85	141.53
500	60.25	330.01

In Figure 34, is shown the trend of the mean phase velocity as a function of frequency, either in the healthy or in the pathologic case.

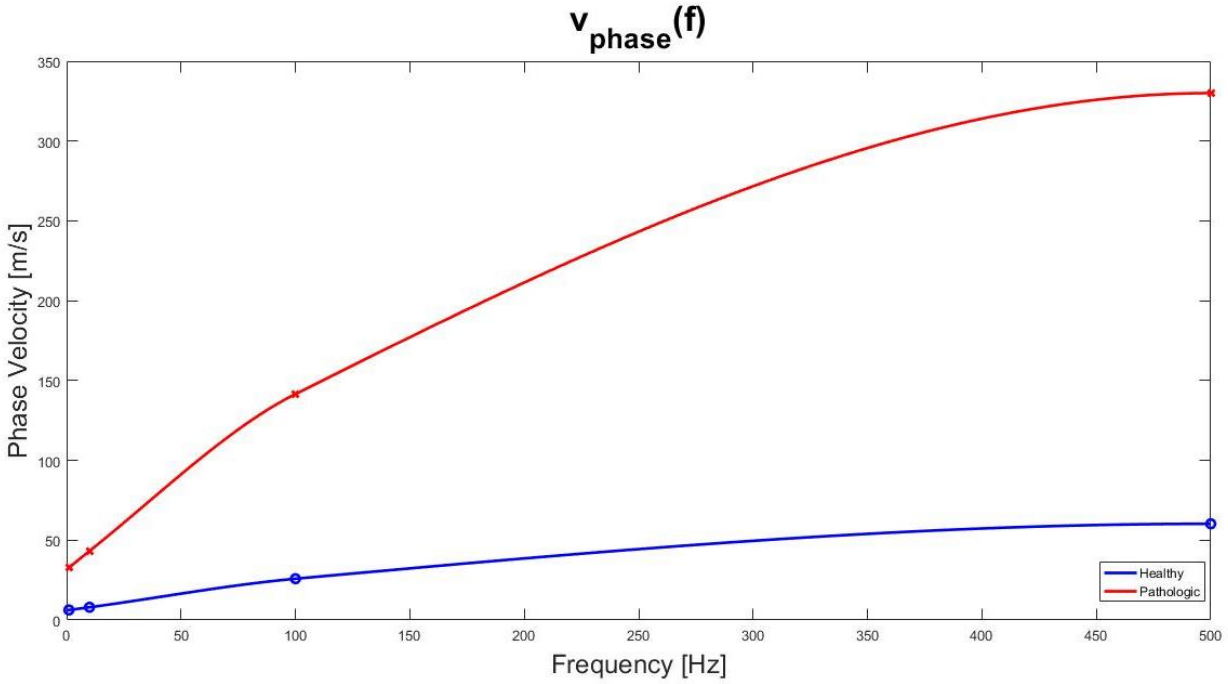

Figure 34-Phase velocity as a function of the frequency, both in healthy and pathologic case

Having the phase velocity at each frequency, allows the computation of the wavelength, which values are reported in TABLE 17 and shown in the plot in Figure 35.

TABLE 17-WAVELENGTH AS A FUNCTION OF THE FREQUENCY

Frequency [Hz]	Phase Velocity [m/s]		Wavelength [m]	
	Healthy	Pathologic	Healthy	Pathologic
1	6.30	32.73	6.30	32.73
10	7.99	43.26	0.80	4.33
100	25.85	141.53	0.26	1.41
500	60.25	330.01	0.12	0.66

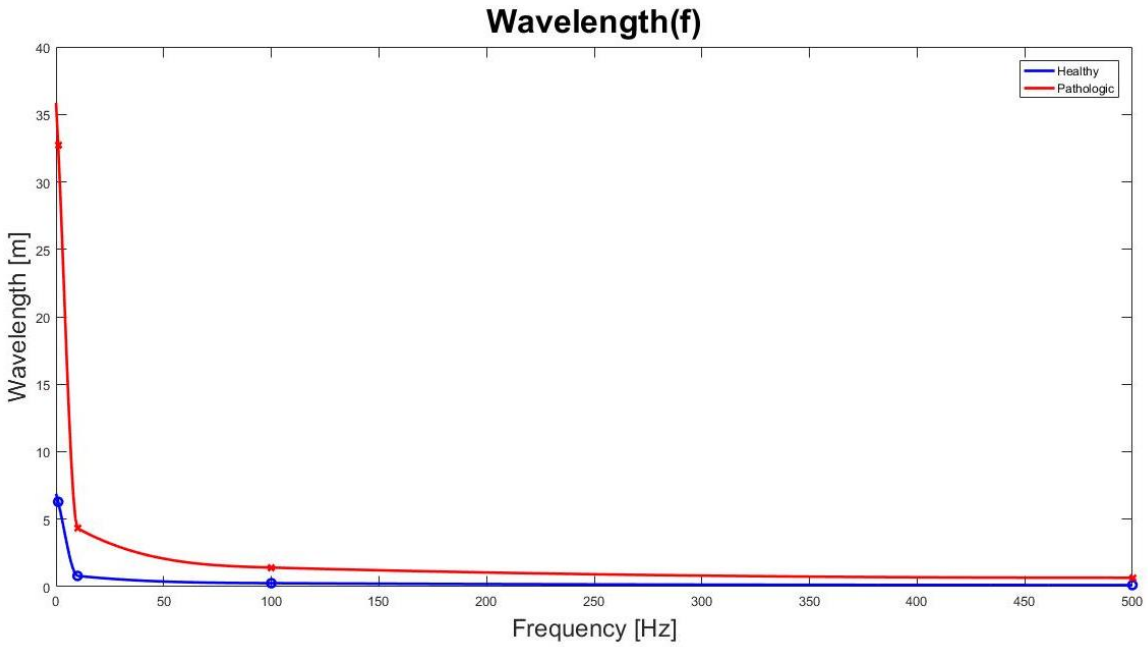

Figure 35-Wavelength as a function of frequency both in healthy and in pathologic case

CHAPTER 6

DISCUSSION

The work carried out in this dissertation focuses on wave propagation in pulmonary circulation and analyzes the response of the system to an input pressure wave of known amplitude and different frequency. The system has been outlined as a one-dimensional waveguide, filled with fluid, and its behavior has been studied in the frequency domain. The response of such a system is strongly influenced by the relative properties of fluid and tube wall and it is related to the energy transfer between the two. A wave propagating in the fluid carries energy, which is either dissipated due to the medium of propagation or transferred to the wall of the waveguide. The energy transfer depends on the impedance mismatch between fluid and tube wall: a higher impedance mismatch implies that the energy is less likely to be transferred to the wall, remaining in the fluid. With a lower impedance mismatch, the energy is transferred more easily from the fluid to the wall. Once transferred, the energy dissipates, depending on the material properties of the wall: in the case of study, the arterial wall is treated as a viscoelastic material, for which behavior has been described with a Voigt model. Recalling the description of a Voigt model, one can characterize the material with the following elastic modulus:

Equation 54-Elastic modulus according to Voigt model

$$E = E_0 + i\omega\eta_w$$

With this choice, one can notice that the higher the frequency, the higher the viscous component (damping). Energy transfer being equal, the higher the frequency, the higher the energy dissipation in the wall. Another important remark on frequency range can be done considering

compliance and inertia, recalling the fact that a transmission line approach is used. The arterial tree consists of several segments, outlined as the transmission line, shown in Figure 36.

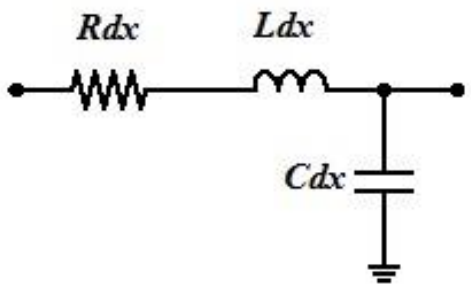

Figure 36-Transmission line for a segment of length dx

Reminding the definition of R, L and C, and the impedance associated, one can write:

Equation 55-Resistance per unit length and relative impedance

$$\begin{cases} R = \dfrac{\rho\omega}{\pi r^2 M}\sin\theta \\ Z_R = R \end{cases}$$

Equation 56-Inertance per unit length and relative impedance

$$\begin{cases} L = \dfrac{\rho}{\pi r^2 M}\cos\theta \\ Z_L = i\omega L \end{cases}$$

Equation 57-Compliance per unit length and relative impedance

$$\begin{cases} C = \dfrac{2(1-v^2)\pi {r_0}^2}{E}\dfrac{r_0}{h} \\ Z_C = \dfrac{1}{i\omega C} \end{cases}$$

From the expression of the impedances, one can notice that impedance relative to the inertance is directly proportional to the frequency, while for the compliance, the impedance is inversely proportional. The lower the frequency, the higher the value of Z_C, the lower the value of Z_L, namely the inductance will act like a short circuit and the compliance as an open circuit. The

higher the frequency, the lower the value of Z_C, the higher the value of Z_L, meaning that the inertance will be an open circuit and the compliance a short circuit. Starting from this, one can conclude that at lower frequency the role of the compliance is predominant, while at higher frequency the inertia contribution is the most relevant.

6.1 Preliminary study

A first simulation of wave propagation has been performed in a simplified pulmonary arterial tree, which considered only three bifurcations, thus seven segments: main pulmonary artery, right and left pulmonary artery, and the four lobar arteries (two upper and two lower). The analytical simulation set up in MATLAB, was then compared to the finite element simulation performed in COMSOL®, in order to validate the analytical model. The results were visualized in terms of both real part of the pressure in [Pa] and magnitude of pressure in [dB]. The analytical and FEM solutions were compared both qualitatively, visualizing the pressure distribution along the arterial tree, and quantitatively, analyzing the relative errors between the two models with regard to the magnitude of the pressure. The mean errors are reported in TABLE 18.

TABLE 18 - MEAN PERCENT ERROR FOR EACH FREQUENCY ANALYZED

Frequency [Hz]	**Mean Percent Error [%]**
1	0.72
5	1.93
10	3.54
15	7.14
50	35.00
100	42.47

A good agreement between the two models was found, both qualitatively and quantitatively. At 100Hz the error is maximum (42.47%) and in general it can be noticed that the higher the frequency is, the higher the error is. Recalling the relationship between wavelength and frequency:

Equation 58-Wavelength as a function of the frequency

$$\lambda = \frac{v_p}{f}$$

At higher frequency, the wavelength becomes shorter and approaches the dimension of the nominal element of the mesh used in the finite element model: this feature may explain the increase of the error with the frequency. From the comparison with the FE model, the analytical model can be considered to be validated. It is also worth making some consideration about the trend of the real part of the pressure, along the tree. The energy of the input wave gets attenuated due to the presence of blood, and it is also transmitted to the arterial wall. Material properties of blood and arterial wall are comparable, thus the impedance mismatch is low and the energy transfer rate between fluid and wall is high. Once in the wall, the energy dissipation depends on the material properties. From the results obtained, it is evident how the higher the frequency, the higher the dissipation, and this is to be related to the frequency-dependent behavior of a viscoelastic material. Increasing the frequency, the viscous component of the arterial wall is dominant with respect to the elastic one, recalling also the fact that a Voigt model has been used. The viscous component is related to damping, so the higher the frequency, the higher the damping in the material, and the attenuation becomes more relevant, as it can be noticed from the plot of the real part of the pressure at different frequencies.

6.2 Pulse wave simulation

The analytical model has also been used to simulate a pulse wave propagating along the arterial tree. It is known how the ventricle contraction generates a pressure pulse that propagates down the blood vessel, being both transmitted and reflected: the typical arterial pressure waveform is related to the interaction between transmitted and reflected waves. By definition, the spectrum of a pulse wave is characterized by different peaks at different frequencies, which constitute the harmonics of the wave; superimposing each of these harmonics, the pulse waveform can be reconstructed. Given a sinusoidal input boundary condition, the developed analytical model can compute a solution: the input sinusoid can be associated to a single harmonic of the pulse wave. Each harmonic constituting the pulse wave spectrum has been used as a boundary condition, and the superposition of each solution gave an idea of the effect of a pulse wave as an input. After obtaining a solution by superposition principle in the frequency domain, it has been transformed in the time domain, and the result is shown in Figure 37.

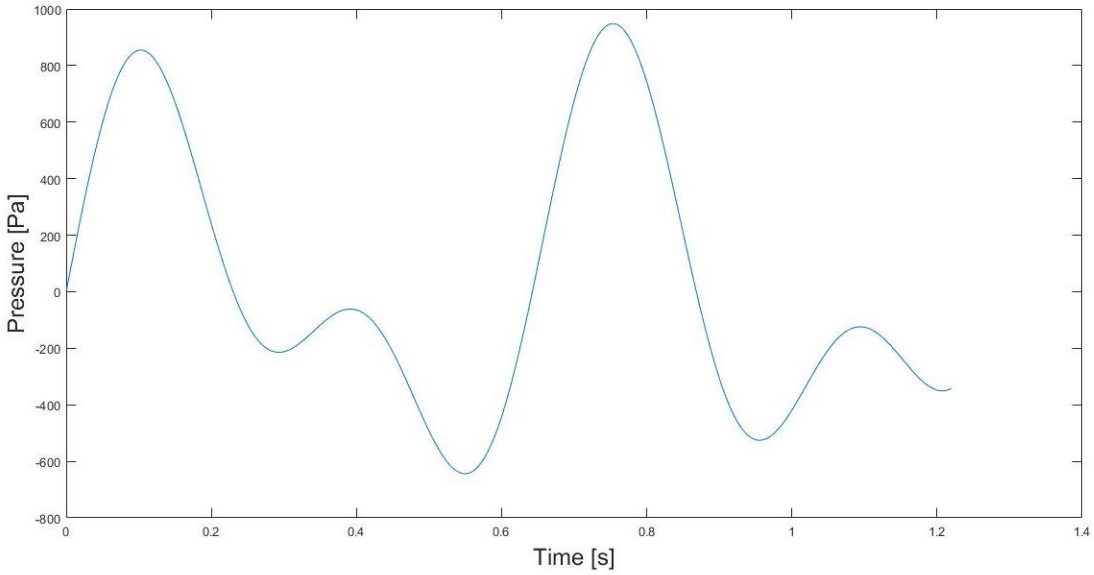

Figure 37-Pulse wave in the time domain

Pulmonary arterial pressure ranges from 15 to 30 mmHg (2.00 – 4.00 kPa) in systole and from 8 to 15 mmHg in diastole (1.07 – 2.00 kPa). The plot reported in Figure 37 shows a pressure ranging from -0.643 to 0.948 kPa (-4.82 – 7.11 mmHg). This discrepancy can be addressed reminding that the analytical model inquires the dynamics of the system, so that the result shows just the pressure fluctuation, neglecting the steady-state component of it. The value of the mean pulmonary artery pressure is in a range between 9 and 18 mmHg (1.20 – 2.40 kPa): a value inside this range must be applied as an offset to the result obtained in the time domain. In Figure 38, it is shown the pulse pressure in the time domain with a chosen offset equal to 13 mmHg (1.73 kPa). It can be noticed that the minimum of this wave is 1.08 Pa (8.17 mmHg) and the maximum is 2.62 kPa (19.64 mmHg), which agrees to the physiological range.

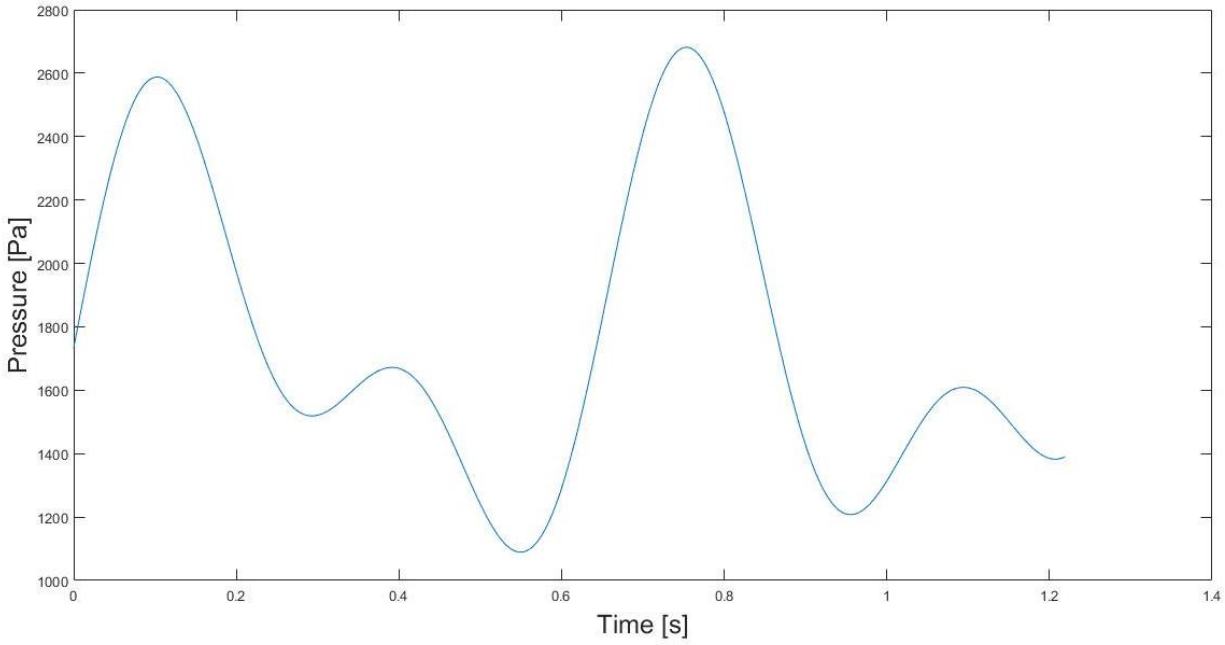

Figure 38-Pressure pulse wave in the time domain, with an offset recalling the mean pulmonary pressure

This result is aimed to show how a solution in the time domain can be reconstructed from the output of the analytical model: the superimposition of solution in terms of pressure in the

frequency domain simulates with a quite a good agreement a pulse wave and it is a suitable tool to obtain information in the time domain as well.

6.3 Pathology simulation

Sickle cell disease and pulmonary hypertension have been taken into consideration during the development of this work and they have been simulated increasing terminal impedance and thickness and elastic modulus of the arteries, mimicking vaso-occlusion, thickening and stiffening processes which characterize the progression of these diseases. Recalling the expression for the vessel compliance, one can notice that it decreases with the increase of both thickness and elastic modulus.

Equation 59-Compliance per unit length

$$C = \frac{2(1-\upsilon^2)\pi {r_0}^2}{E}\frac{r_0}{h}$$

It is evident how these structural and mechanical changes imply that the pulmonary arterial wall becomes less compliant, thus more rigid, and that the impedance mismatch between arterial wall and the fluid increases. An increase in the impedance mismatch causes in turn a decrease in the rate of energy transfer between the arterial wall and the fluid, which can be related to a higher penetration of the real part of the pressure down the arterial tree: this behavior matches with the results obtained. In fact, being the frequency equal, one can notice that in the pathological case, the real part of the pressure penetrates further down in the tree with respect to the healthy case. Values of phase velocity have been computed too, according to what reported by Wiener et al. [1].

Equation 60-Phase velocity

$$v_p = \frac{\omega}{\beta}$$

Where:

- ω = angular frequency;
- β = imaginary part of propagation coefficient γ.

At the frequencies taken into consideration, the computed values of phase velocity are higher in the pulmonary hypertension case, and this can be explained recalling the Moens-Kortweg equation.

Equation 61-Moens-Kortweg equation

$$v_p^2 = \frac{Eh}{2\rho r}$$

The Moens-Kortweg equation reported above, shows how phase velocity is directly proportional to the square root of elastic modulus and thickness and inversely proportional to the square root of the radius. It is worth reminding that pulmonary hypertension has been simulated with an increase in thickness of the arterial wall, and a consequent decrease in radius, and an increase in the elastic modulus. Starting from the above consideration, it is evident how phase velocity is found to be higher in the pulmonary hypertension simulation. Phase velocity is also directly proportional to wavelength, so the higher the phase velocity is, the higher the wavelength is: the PH case is characterized by higher wavelength with respect to the healthy case.

6.4 Limitations

In this thesis, the pulmonary circulation has been modeled as a one-dimensional branching waveguide with the purpose of inquiring the pressure wave propagation and some limitations can be reported. First of all, in the attempt of outlining the pulmonary circulation structure, the geometry used as an input for the analytical model presents some strong approximation. Seven segments were considered in the geometry used, representing respectively the main pulmonary

artery, the right and left pulmonary artery, and the four lobar arteries. Each of these segments was considered to be straight and was characterized by one value of radius, length, and thickness. Pulmonary arteries are not straight, but they curve to fit the anatomical space available during their path. Tapering, namely the decrease of the diameter from input to output of a single segment, is another typical feature of pulmonary arteries, especially main, right and left pulmonary arteries. Each segment constituting the arterial tree, has been modeled as a straight cylinder in the current work, so either curvature and tapering have been neglected. The values of thickness have been computed setting a constant radius-to-thickness ratio, since no anatomical data were found in literature, and this constitutes another approximation. Arterial wall mechanical properties have been modeled with a Voigt-model, thus as to be linearly viscoelastic: non-linear mechanical behavior of arteries has not been considered in the current work. Only seven segments constitute the large arteries of the model, whereas all the remaining segments have been considered small arteries, thus approximated with morphometric data. Therefore, this study should be considered a preliminary evaluation of the performance of the one-dimensional waveguide to a case of study such as the pulmonary circulation. Another limitation is the simulation of pathology. As far as sickle cell disease is concerned, terminal impedances have been increased of an arbitrary factor to reproduce vaso-occlusion. Moreover, the mechanical and structural changes introduced in the analytical model to simulate pulmonary hypertension are only qualitative. Thickness, stiffness, and radius have been modified in an arbitrary way to reproduce the progression of the disease: no experimental data have been used for simulating the pathology.

6.5 Future developments

Starting from the limitations reported in Paragraph 6.4, the work carried out in this thesis showed some preliminary results and possible application of an analytical model aimed at the analysis of wave propagation: as such, it can be further developed for having a wider and more accurate comprehension of the phenomenon. An experimental stage could be of particular interest for mainly two reasons. First of all, most of the data used come from literature, such as arterial material properties, or are approximations, like the radius-to-thickness ratio and pulmonary hypertension remodeling. An *ex-vivo* mechanical characterization of pulmonary arteries could be a first step for having a better analysis, together with a morphometric study for obtaining more accurate values of thickness of the vessels, both for healthy and pulmonary hypertension case. Secondly, an experimental validation, namely comparing values computed with the analytical model with experimental ones, could be more meaningful than a FE validation. As pointed out in Section 6.4, the developed model does not simulate the entire arterial network by now, since it considers only seven segments. In order to overcome this limitation, the inclusion of further branches should be considered for having a more physiological model. Another interesting development could be considering the whole pulmonary circulation, coupling arterial and venous tree with the capillary sheet. Pulmonary vascular resistance is strongly affected by the contribution of pulmonary vein [32], so considering arteries only limits the completeness of the model.

6.6 Conclusions

The focus of the current dissertation was the development of a model to study the wave propagation in the pulmonary circulation and its application on a pathological case, such as pulmonary hypertension. A frequency domain approach was used, based on the electrical

analogue of the transmission line. The choice of working in the frequency domain was related to the fact that in this case the system is treated as linear and the solution is found via the superposition principle: this approach is less computationally demanding with respect to the time domain one, and allows the direct incorporation of viscoelasticity [26]. A structured-tree outflow boundary condition was used: lumped parameters models (pure resistors, Windkessel, …) have not been taken into consideration since the impossibility of simulating wave propagation in the region they model [2]. Three main parts comprise the present work:

1. A preliminary study, in which the analytical model has been validated with respect to a finite element model;
2. A pulse wave simulation, in which a pressure pulse has been simulated via superposition of different harmonics;
3. Pulmonary hypertension simulation, in which structural and mechanical changes have been introduced in the model with the aim of simulate the effect of the pathology.

The results of the preliminary study (point 1) show that the solution of the analytical model is in good agreement with the finite element model: a suitable tool is thus provided for further simulation. The main advantage of an analytical model with respect to a finite element model is related to the computational time and effort. The computation of the analytical solution takes a time of the order of 20-30 seconds, whereas the finite element simulation in COMSOL® computes the solution in approximatively 5-6 minutes, for a single frequency. The pulse wave simulation (point 2) shows the versatility of the approach chosen for the analytical model. The arterial pulse is mathematically complex, due to multiple frequencies constituting its spectrum; the analysis of its single components is easier, since simple sinusoids are considered as input for the system, and the superposition principle represents a suitable method to reconstruct a complex

solution. As explained before, the progression of pulmonary hypertension causes mechanical and structural changes, such as thickening and stiffening, which can affect wave propagation. The results of the pathology simulation (point 3) have shown changes in pressure distribution along the arterial tree and changes in the phase velocity, which can be relevant in a clinical perspective.

This work showed that a frequency-domain approach based on one-dimensional waveguide modeling gives promising results in terms of pressure wave propagation. The pathology simulation gave reasonable results, showing changes in the pressure distribution, thus the validity of the approach in a clinical perspective. In conclusion, this model is a versatile, suitable and time-saving tool for different application, that can be further developed with the aim of obtaining diagnostically relevant information and a better knowledge of disease processes related to pathologies, such as sickle-cell disease and pulmonary hypertension.

CITED LITERATURE

[1] F. Wiener, E. Morkin, R. Skalak, and a. P. Fishman, "Wave Propagation in the Pulmonary Circulation," *Circ. Res.*, vol. 19, no. 4, pp. 834–850, 1966.

[2] M. S. Olufsen, C. S. Peskin, W. Y. Kim, E. M. Pedersen, A. Nadim, and J. Larsen, "Numerical simulation and experimental validation of blood flow in arteries with structured-tree outflow conditions," *Ann. Biomed. Eng.*, vol. 28, no. 11, pp. 1281–1299, 2000.

[3] M. Thiriet, *Anatomy and Physiology of the Circulatory and Ventilatory*. 2013.

[4] G. J. Tortora and M. T. Nielsen, *Principles of Human Anatomy*, vol. 53, no. 9. 2012.

[5] G. Anastasi *et al.*, *Anatomia Umana - Trattato - volumi 1-3*. 2006.

[6] H. Murillo, M. J. Cutalo, R. P. Jones, M. J. Lane, D. Fleischmann, and C. S. Restrepo, "Pulmonary Circulation Imaging: Embryology and Normal Anatomy," *Semin. Ultrasound, CT MRI*, vol. 33, no. 6, pp. 473–484, 2012.

[7] Y. Fung, *Biomechanics: Circulation*. Springer, 1997.

[8] D. C. Rees, T. N. Williams, and M. T. Gladwin, "Sickle-cell disease," *Lancet*, vol. 376, no. 9757, pp. 2018–2031, 2010.

[9] E. S. Klings *et al.*, "An official american thoracic society clinical practice guideline: Diagnosis, risk stratification, and management of pulmonary hypertension of sickle cell disease," *Am. J. Respir. Crit. Care Med.*, vol. 189, no. 6, pp. 727–740, 2014.

[10] M. T. Gladwin, "Cardiovascular complications and risk of death in sickle-cell disease," *Lancet*, vol. 387, no. 10037, pp. 2565–2575, 2016.

[11] J. I. E. Hoffman, "Pulmonary Hypertension in Sickle Cell Disease," *N. Engl. J. Med.*, vol. 365, no. 17, pp. 1645–1649, Oct. 2011.

[12] M. Gladwin, V. Sachdev, M. Jison, Y. Shizukuda, J. Plehn, and K. Minter, "Pulmonary hypertension as a risk factor for death in patients with sickle cell disease.," *N Engl J Med.*, vol. 350, no. 9, pp. 886–95, 2004.

[13] L. M. De Castro, J. C. Jonassaint, F. L. Graham, A. Ashley-Koch, and M. J. Telen, "Pulmonary hypertension associated with sickle cell disease: Clinical and laboratory endpoints and disease outcomes," *Am. J. Hematol.*, vol. 83, pp. 19–25, 2008.

[14] K. I. Ataga *et al.*, "Pulmonary hypertension in patients with sickle cell disease: a longitudinal study.," *Br. J. Haematol.*, vol. 134, no. 1, pp. 109–15, 2006.

[15] B. Oswaldo Castro *et al.*, "The Acute Chest Syndrome in Sickle Cell Disease: Incidence and Risk Factors and The Cooperative Study of Sickle Cell Disease."

[16] N. Galiè *et al.*, "2015 ESC/ERS Guidelines for the diagnosis and treatment of pulmonary hypertension," *Eur. Heart J.*, vol. 37, no. 1, pp. 67–119, Jan. 2016.

[17] E. Bossone *et al.*, "Echocardiography in pulmonary arterial hypertension: From diagnosis

CITED LITERATURE (continued)

to prognosis," *J. Am. Soc. Echocardiogr.*, vol. 26, no. 1, pp. 1–14, 2013.

[18] V. O. Kheyfets, W. O'Dell, T. Smith, J. J. Reilly, and E. a Finol, "Considerations for numerical modeling of the pulmonary circulation--a review with a focus on pulmonary hypertension.," *J. Biomech. Eng.*, vol. 135, no. 6, pp. 61011–15, 2013.

[19] M. M. Hoeper *et al.*, "Definitions and diagnosis of pulmonary hypertension," *J. Am. Coll. Cardiol.*, vol. 62, no. 25 SUPPL., pp. D42–D50, 2013.

[20] N. Chesler and Z. Wang, "Pulmonary vascular wall stiffness: An important contributor to the increased right ventricular afterload with pulmonary hypertension," *Pulm. Circ.*, vol. 1, no. 2, p. 212, 2011.

[21] M. Humbert *et al.*, "Cellular and molecular pathobiology of pulmonary arterial hypertension," *J. Am. Coll. Cardiol.*, vol. 43, no. 12, pp. S13–S24, 2004.

[22] D. B. Badesch *et al.*, "Diagnosis and Assessment of Pulmonary Arterial Hypertension," *J. Am. Coll. Cardiol.*, vol. 54, no. 1 SUPPL. 1, pp. S55–S66, 2009.

[23] M. M. Hoeper *et al.*, "Complications of Right Heart Catheterization Procedures in Patients With Pulmonary Hypertension in Experienced Centers," *J. Am. Coll. Cardiol.*, vol. 48, no. 12, pp. 2546–2552, 2006.

[24] K. Bennell, F. Dobson, and R. Hinman, "Measures of physical performance assessments: Self-Paced Walk Test (SPWT), Stair Climb Test (SCT), Six-Minute Walk Test (6MWT), Chair Stand Test (CST), Timed Up & Go (TUG), Sock Test, Lift and Carry Test (LCT), and Car Task," *Arthritis Care Res. (Hoboken).*, vol. 63, no. S11, pp. S350–S370, Nov. 2011.

[25] J. Womersley, "An elastic tube theory of pulse transmission and oscillatory flow in mammalian arteries," 1957.

[26] P. Segers, N. Stergiopulos, P. Verdonck, and R. Verhoeven, "Assessment of distributed arterial network models," *Med. Biol. Eng. Comput.*, vol. 35, no. 6, pp. 729–736, Nov. 1997.

[27] E. O. Attinger, "Pressure transmission in pulmonary arteries related to frequency and geometry.," *Circ. Res.*, vol. 12, pp. 623–41, Jun. 1963.

[28] G. H. Pollack, R. V. Reddy, and A. Noordergraaf, "Input Impedance, Wave Travel, and Reflections in the Human Pulmonary Arterial Tree: Studies Using an Electrical Analog," *IEEE Trans. Biomed. Eng.*, vol. BME-15, no. 3, pp. 151–164, 1968.

[29] W. R. Milnor, C. R. Conti, K. B. Lewis, and M. F. O'Rourke, "Pulmonary Arterial Pulse Wave Velocity and Impedance in Man," *Circ. Res.*, vol. 25, no. 6, 1969.

[30] A. P. Avolio, "Multi-branched model of the human arterial system," *Med. Biol. Eng. Comput.*, vol. 18, no. 6, pp. 709–718, 1980.

CITED LITERATURE (continued)

[31] R. L. Spilker, J. A. Feinstein, D. W. Parker, V. M. Reddy, and C. A. Taylor, "Morphometry-based impedance boundary conditions for patient-specific modeling of blood flow in pulmonary arteries," *Ann. Biomed. Eng.*, vol. 35, no. 4, pp. 546–559, 2007.

[32] M. U. Qureshi *et al.*, "Numerical simulation of blood flow and pressure drop in the pulmonary arterial and venous circulation," *Biomech. Model. Mechanobiol.*, vol. 13, no. 5, pp. 1137–1154, 2014.

[33] E. Attinger, *Pulsatile blood flow proceedings. E.O. Attinger, editor.* New York: McGraw-Hill, 1964.

[34] T. Inajima *et al.*, "Relation between blood pressure estimated by pulse wave velocity and directly measured arterial pressure," *J. Robot. Mechatronics*, vol. 24, no. 5, pp. 811–819, 2012.

[35] T. Pereira, C. Correia, and J. Cardoso, "Novel methods for pulse wave velocity measurement," *J. Med. Biol. Eng.*, vol. 35, no. 5, pp. 555–565, 2015.

[36] S. Singhal, R. Henderson, K. Horsfield, K. Harding, and G. Cumming, "Morphometry of the Human Pulmonary Arterial Tree," *Circ. Res.*, vol. 33, no. 2, pp. 190–197, 1973.

[37] A. N. Strahler, "Quantitative analysis of watershed geomorphology," *Trans. Am. Geophys. Union*, vol. 38, no. 6, p. 913, 1957.

[38] W. W. Nichols, W. W. Nichols, and D. A. McDonald, *McDonald's blood flow in arteries : theoretical, experimental and clinical principles.* Hodder Arnold, 2011.

[39] H. Hasegawa and H. Kanai, "Measurement of elastic moduli of the arterial wall at multiple frequencies by remote actuation for assessment of viscoelasticity," *Japanese J. Appl. Physics, Part 1 Regul. Pap. Short Notes Rev. Pap.*, vol. 43, no. 5 B, pp. 3197–3203, 2004.

VITA

NAME:	Andrea Carmignotto
EDUCATION:	L.T., Ingegneria Biomedica, Politecnico di Milano, Milan, Italy, 2015
	Higher Education, Liceo Scientifico Niccolò Machiavelli, Pioltello, Italy, 2012
RESEARCH EXPERIENCE:	01/2017 - 05/2017 Research Assistant in the Acoustics and Vibrations Laboratory (AVL) at University of Illinois at Chicago
	02/2015 – 07/2015 Research in the Laboratory of Biological Structures Mechanics (LaBS) at Politecnico di Milano
	02/2014 – 09/2014 Activity in the Novel, Emerging Computer System Technology Laboratory (NECST) at Politecnico di Milano